DISSERTATIONES PHYSICAE UNIVERSITATIS TARTUENSIS

51

DISSERTATIONES PHYSICAE UNIVERSITATIS TARTUENSIS
51

ELECTROMECHANICAL CHARACTERIZATION OF IONIC POLYMER-METAL COMPOSITE SENSING ACTUATORS

ANDRES PUNNING

TARTU UNIVERSITY
PRESS

The study was carried out at the University of Tartu, Estonia.

The Dissertation was admitted on June 15, 2007, in partial fulfillment of the requirements for the degree of Doctor of Philosophy in physics (applied physics), and was allowed for defence by the Council of the Department of Physics, University of Tartu.

Supervisors: Prof. Alvo Aabloo, University of Tartu, Estonia
Maarja Kruusmaa, Ph.D , University of Tartu, Estonia

Opponents: Prof. Kwang J. Kim, University of Nevada, Reno, USA
Ergo Nõmmiste, Ph.D , University of Tartu, Estonia

Defence: August 08, 2007 at the University of Tartu, Estonia

ISSN 1406–0647
ISBN 978–9949–11–646–1 (trükis)
ISBN 978–9949–11–647–8 (PDF)

Autoriõigus Andres Punning, 2007

Tartu Ülikooli Kirjastus
www.tyk.ee
Tellimuse nr 227

CONTENTS

LIST OF PUBLICATIONS

This Thesis is a summary based on the following papers, which are referred to in this text by their Roman numerals:

I. **Surface resistance experiments with IPMC sensors and actuators.** A. Punning, M. Kruusmaa, A. Aabloo, Sensors and Actuators A: Physical, 133/1, 2007, pp. 200–209.
II. **A Self-Sensing Ionomeric Polymer Metal Composite (IPMC) Actuator.** A. Punning, M. Kruusmaa, A. Aabloo, Sensors and Actuators A: Physical, 136/2, 2007, pp. 656–664.
III. **A Distributed Electromechanical Model of Ionomeric Polymer Metal Composite (IPMC).** A. Punning, U. Johanson, M. Anton, A. Aabloo, M. Kruusmaa, Sensors and Actuators A: Physical, in Print.
IV. **Empirical model of a bending IPMC actuator.** A. Punning, M. Anton, M. Kruusmaa, A. Aabloo, Smart Structures and Materials 2006: Electroactive Polymer Actuators and Devices (EAPAD); San Diego, California, USA; 27.02.–02.03.2006. Bellingham: SPIE, 2006, (Proceedings of SPIE – The International Society for Optical Engineering), 61681V.
V. **Selfsensing actuator**, PCT Patent application, 08.03.2006, Tartu University; P200600005, Authors: Andres Punning, Maarja Kruusmaa, Alvo Aabloo.

Other publications, relevant to my work but not included in this Thesis:

VI. **Validating Usability of Ionomeric Polymer-Metal Composite Actuators for Real Life Applications.**: M. Anton, A. Punning, A. Aabloo, M. Kruusmaa, (2006). IROS 2006, IEEE/RSJ International Conference on Intelligent Robots and Systems; Beijing, China; 9–15 October, 2006. IEEE, 2006.
VII. **Towards a biomimetic EAP robot. Towards Autonomous Robotic Systems (TAROS 2004);** M. Anton, A. Punning, A. Aabloo, M. Listak, M. Kruusmaa, Clochester, UK; 06.–08.19.2004. Clochester, UK: University of Essex, 2004, (Technical Report Series), 1–7.
VIII. **A Biologically Inspired Ray-like Underwater Robot with Electroactive Polymer Pectoral Fins.** A. Punning, M. Anton, M. Kruusmaa, A. Aabloo, IEEE Confrence "Mechatronics and Robotics 2004" (MechRob04); Aachen, Germany; 13.–15.09.2004. Aachen: Eysoldt, 2004, (2), 241–245.
IX. **Linked manipulator with a short link of electroactive polymer material**, Estonian Patent application, 08.03.2006, Tartu University; P200600005, Authors: Maarja Kruusmaa, Mart Anton, Andres Punning, Alvo Aabloo.

ABSTRACT

Ionic Polymer-Metal Composites (IPMC) are electroactive polymer materials that bend in response to electric stimulation. A typical IPMC is an ion exchange polymer membrane covered with metal layer on both sides. An IPMC bends when voltage is applied between the metallized faces of the membrane. IPMC exhibits relatively large bending, but relatively low force in response to the voltage of only a few volts. There also exists a reverse effect: during bending caused by an external force, voltage is generated between the metallized faces of the membrane. Both electromechanical effects are caused by movement of charged particles inside the membrane.

This work introduces a model of an IPMC as a distributed one-dimensional RC transmission line. The circuit elements of the transmission line have clear physical interpretations – the conductivity of the electrodes, the pseudo-capacitance of the double-layer forming at the boundary of the electrodes, the electric current caused by electrolysis etc. Due to the non-zero resistance of the electrodes and the large capacitance of the polymer membrane, it is obvious that the electric current and voltage drops in an IPMC device will be remarkable and the distribution of the electrical parameters is not uniform. This causes the non-uniform mechanical response. The distributed nature of the model described in the current work permits predicting the non-uniform bending of the IPMC actuators in time domain. Likewise, the distributed model helps to reconcile the output of an IPMC-based position sensor with its shape.

This thesis describes how the electrical parameters are measured and presented, how the mechanical parameters of the bending actuator are obtained and how these results are later combined togheter. When the measurable electrical parameters and the changing shape of IPMC are described in a specific distinctive way, the correlation between the bending motion and electrical parameters is apparent. In the model, described in this work, the electromechanical coupling between the electrical parameters and bending motion is expressed by means of distribution of electric current along the material in time domain.

Furthermore, taking into account several nonlinear parameters, the model is consistent with the experimental results even when the inflexion of the actuator or sensor is large or the water electrolysis appears. The considered causes of nonlinearity are the changing conductivity of the electrodes of IPMC and the electrochemical reactions at the electrodes. In this work the effect of each parameter is illustrated with simulations obtained with Matlab Simulink or with the closed-form solutions of differential equations.

Exploiting the correlation between the resistance and flexure of the electrodes of the IPMC, allows to develop an actuating-sensing device, capable of feeling its own motion.

This work is terminated with a demonstration of a IPMC-based actuating device with more than one pair of input contacts. Taking into account the effect of the changing resistance of the bending surface electrodes, it is possible to gain a complicated flexion of a single-piece IPMC actuator.

1. INTRODUCTION

This thesis presents a model of an IPMC. An IPMC is modeled as a distributed RC transmission line. Unlike other electromechanical models of IPMC materials, the distributed nature of this model permits predicting the non-uniform bending of the material. Instead of modeling the deflection of the tip of a cantilevered IPMC actuator or sensor without taking an interest in the shape of the device between the tip and the input contacts, this model describes the uneven changing flexure of the device. The model makes it possible to describe the distribution of the voltage and electric current in spatial domain and in time-domain. The electromechanical coupling between the electrical parameters and bending motion is implemented by means of the distribution of electric current, particularly the movement of charged particles inside the material. Likewise, the distributed model helps to reconcile the output of an IPMC-based position sensor with the shape.

Furthermore, taking into account several nonlinear parameters, the model is consistent with the experimental results even when the inflexion of the actuator or sensor is large.

Exploiting the nonlinear parameters, especially the correlation between the resistance and flexure of the electrodes of the IPMC, allows to develop an actuating-sensing device, capable of feeling its own motion.

The rest of this thesis is organized as follows. The chapter at hand gives an overview of IPMC materials and the state-of-the-art of their modeling. In the end of this chapter I define my contribution with respect to the related work.

Chapter 2 describes the methodology used to develop and verify the consistency of the model.

Chapter 3 is devoted to the distributed model of IPMCs and Chapter 4 discusses the improvement of the model taking into account the nonlinear effects emerging during actuation. Chapter 5 discusses the model from the point of view of IPMC sensors.

Chapter 6 explains the parameter identification methods to determine the characteristics of the material used in the experiments and Chapter 7 discusses the nonlinear model with electrode reactions.

Chapters 8 and 9 are devoted to implications of the theoretical work described in this thesis. Namely, I described two novel devices, a self-sensing actuator and S-actuator that are developed based on these theoretical results.

1.1. A brief overview of IPMCs

A typical Ionomeric Polymer Metal Composite material bends in response to electrical stimulation (Fig. 1.1). It is an ion exchange polymer membrane covered with metal layer on both sides. The metal layers serve as electric contacts. During the fabrication the membrane is saturated with a certain solvent and ions. Voltage applied between the conductive electrodes causes migration of the ions in the solvent inside the polymer matrix. That in turn leads to non-uniform distribution of the ions inside the polymer. As a result, the material deforms – bends.

There exists also a reverse effect that makes it possible to exploit an IPMC as a mechanical position sensor: during bending caused by an external force, voltage is generated between the two faces of the membrane. Both electromechanical effects are caused by electrochemical effects – the movement of charged particles inside the membrane [1–5].

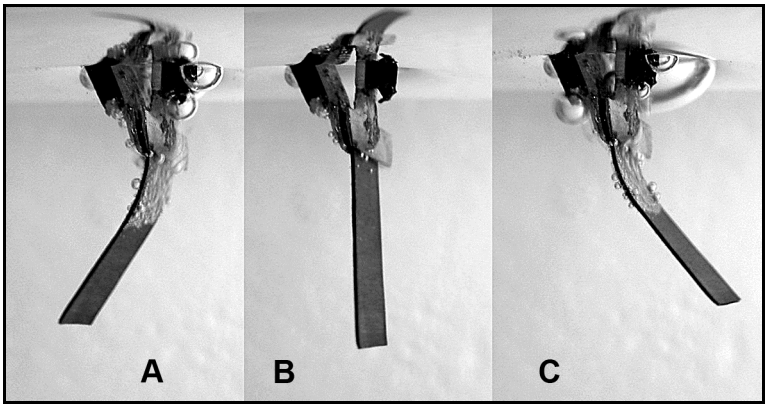

Figure 1.1. An IMPC sheet in a bent configuration with the opposite driving voltage polarity (A and C) and an initial configuration with no electric stimulus applied (B).

In the literature, IPMC (*Ionic* Polymer-Metal Composite, or *Ionomeric* Polymer-Metal Composite) is also called ICPF (Ionic Conducting Polymer Film or Ionic Conducting Polymer gel Film), SPM (Solid Polymer Electrolyte Membrane), IPT (Ionic Polymer Transducer) and IMPC (Ionic Metal-Polymer Composite).

1.2. Actuation of IPMCs

In 1992, Oguro et al. described the actuation function of the IPMC by demonstrating that the material bends when voltage is applied [6]. The sensing effect of an IPMC was found almost at the same time – Sadeghipour et al. introduced their "smart"-material based accelerometer in 1992 [7]. Although the effect of actuation of an IPMC is known over a decade already, the discussion on the actuation mechanism is still ongoing [8, 9, 10]. All theories assume that the deformation of an IPMC is caused by the moving particles inside the solvent-swollen backbone of the polymer.

The backbone of an IPMC is a hydrophobic fluorocarbon polymer sheet with fixed, hydrophilic anion groups. The backbone is highly swollen with a solvent – water or ionic liquid. During the fabrication of the material the proton connected to the terminal group (the chemical unit at the end of a side chain of the polymer), is replaced with a cation. These cations dissociate in water and form an excess of free cations in the hydrated polymer. The remaining polymer chains will have negative charge. There exist two distinct paradigms differently explaining the influence of the moving ions in the course of the actuation of an IPMC:

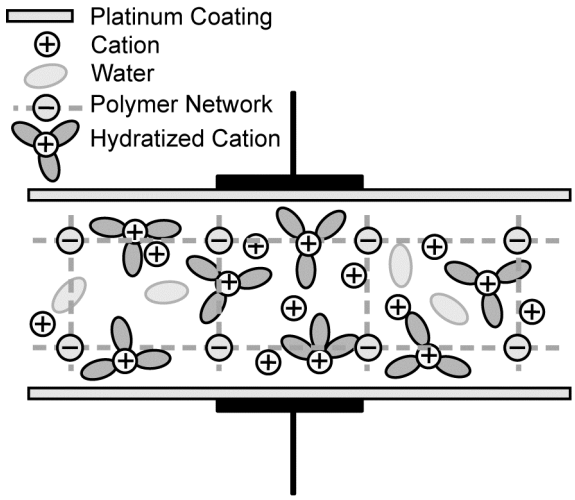

Figure 1.2. An IPMC with no voltage applied.

1. The main cause of deformation of the material is the irregular density of solvent and ions generated by the electric stimulus. The originated free cations hydratize – the molecules of solvent connect to the cations, as shown in Fig. 1.2. When electric field is applied between the faces of the IPMC, the hydrated cations move in the fixed network of negative charged backbone of the polymer towards the negatively charged surface, causing expansion of

the polymer at one face and shrinking at the opposite face. Figuratively, while one face of IPMC withers and shrinks, the opposite face protracts due to swelling with water and ions. As the result, the polymer network bends towards the shrinking face as shown in Fig. 1.3. A theory taking into account the hydratization of cations is proposed in 2000 by DeGennes et al. [8] and by Asaka and Oguro [11].

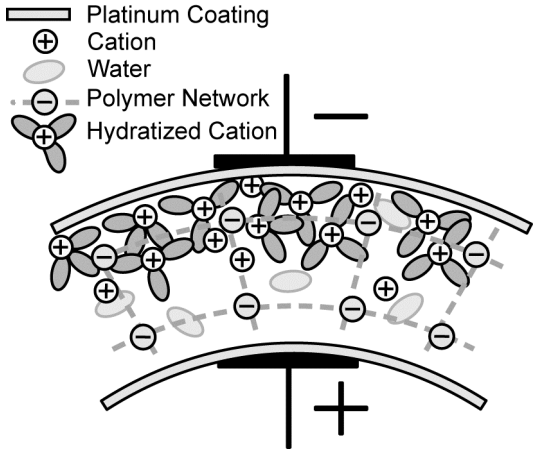

Figure 1.3. The IPMC bends, when DC voltage is applied.

2. When electric field is applied between the faces of an IPMC, the cations move in the fixed network of negative ions of the polymer backbone towards the negatively charged surface. The main cause of deformation of the material is the electrostatic forces of displaced ions. The water is only a passive component influencing the stiffness of the polymer network. A thorough electrostatic model of an IPMC is proposed by Nemat-Nasser and Li [9].

It is plausible that both mechanisms act concurrently and their relative importance depends on the solvent and ions used in the particular case [2].

It must be pointed out that in the described model the ionomer is a *cation exchange membrane*, for instance Nafion^{TM} [12]. If the ionomer is an *anion exchange membrane*, the percolating ions are anions, the fixed network is positively charged and the material bends in the opposite direction.

The ionic polymer actuator bends in the opposite direction if the voltage is reversed. It is possible to gain electrically controllable deformation changes by changing the voltage between the faces of the actuator [2].

The amplitudes of the voltages capable of bending the material are usually a few volts.

1.3. Sensorial properties of IPMCs

Sensing properties of IPMCs were discovered by Sadeghipour et al. in 1992 [7]. They demonstrated that the voltage produced by a small cantilever constructed from Nafion^{TM} was proportional to the acceleration. They proposed usage of IPMCs for vibration sensors.

When the material is mechanically bent, the solvent carrying the free ions is forced towards the region with the lower pressure, like depiced in Fig. 1.3. The distribution of the charges with respect to the neutral axis of the membrane is inflected. An excess of positive charges will occur on the expanding side and a deficit of positive charges will occur on the contracting side of the fixed network of negatively charged polymer backbone. This phenomenon produces a voltage signal that can be detected at the metal electrodes [2, 13, 14].

The reported voltage amplitude is up to some tens of millivolts [4] and the sensing current is reported being a few microamperes [14]. According to the experiments carried out by myself, the output voltages of IPMC sensors were few millivolts (see **I** and **II)**.

When compared to the amount of research on IPMC actuators, there is noticeable less research done on modeling the sensing properties of IPMCs. Newbury et al. presented a scalable model for IPMC actuators and sensors described hereinafter [15]. The model was further elaborated and verified by Bonomo el al. [16]. Farinholt et al derived the charge sensing response for a cantilevered IPMC beam under a step change in tip displacement [17].

The sensing property is proposed to be exploited for energy harvesting from ambient vibrations. Although the acquired power is small, the ionic polymers are able to discharge energy across a load proving that they are capable of supplying power [18].

1.4. Electromechanical models of IPMCs

Although the actuating and sensing properties of IPMCs are known over a decade, the rationale of IPMC sensing and actuating mechanisms are not thoroughly understood. This makes it difficult to predict the behavior of this material and therefore limits the potential applications areas. Several models are proposed so far to model the behavior of IPMC sensors and actuators.

Generally the models represent an IPMC actuator in a cantilever configuration – one end fixed between a clamp serving as the input contacts as depicted in Fig. 1.1 and Fig. 2.1.3. The input parameters of the models of the actuators are usually the input voltage or current, the output parameters are the displacement of the free tip of the actuator and/or the force generated by the tip. For the models of sensors the commonly used input parameters are the position,

speed or acceleration of the tip; the output parameters are usually the voltage or electric current at the electrodes located at one end of the strip.

The nomenclature of the models presented here is not complete. The purpose of this short overview is only to demonstrate the variety of possibilities of modeling the electromechanical properties of the material.

Empirical models

Historically, the first model of an IPMC was probably developed by Kanno et al in 1994 – only two years after the discovery of the actuation phenomenon of the IPMC [10]. The model described the mechanical response of a cantilevered actuator to a step voltage input. The equation characterizing the motion of the tip of the actuator was a sum of exponentials:

$$Y = A \cdot e^{-\alpha t} + B \cdot e^{-\beta t} + C \cdot e^{-\gamma t} + D \cdot e^{-\delta t} + E \tag{1.1}$$

The 9 parameters – constants A, B, C, D, E and time coefficients $\alpha, \beta, \gamma, \delta$ were determined by curve-fitting the experimental results.

Newbury and Leo [15, 19, 20] propose a linear two-port model that can be used for modeling both actuation and sensing properties of a cantilever actuator or sensor. The energy conversion between the electric and mechanical domains can be represented using an ideal linear transformer, where the electric quantities are shown on one side of the transformer, and the mechanical quantities are on the other side as shown in Fig. 1.4.

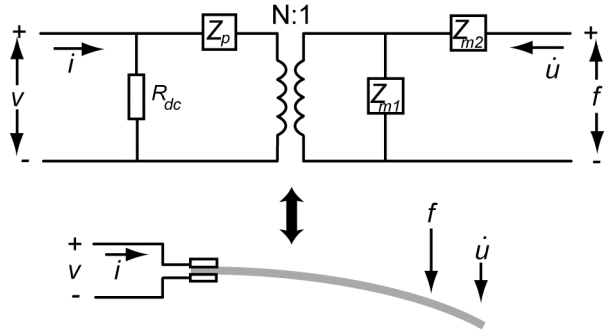

Figure 1.4. The model of Newbury and Leo.

There are two mechanical terms in this model – mechanical impedance due to stiffness and inertia of the cantilever beam – and two electric terms (DC resistance and charge storage).

Lumped models

Several authors have described their models of the IPMC in a form of a lumped electrical equivalent circuit where the input parameters – voltage, or current – are converted to the output parameters – tip displacement, force or power – using the methods of solving electrical circuits and coupling the electrical parameters with mechanical and spatial parameters.

Jung et al. investigate the response of a bulk of the IPMC in a frequency domain and describe the results as a lumped high pass filter as shown in Fig. 1.5. [21].

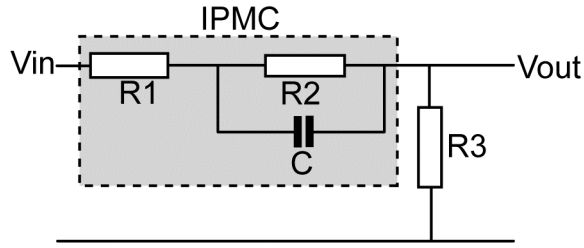

Figure 1.5. Jung's model.

The frequency response of such a filter is described by the formula containing experimentally derived values of resistors and capacitors:

$$G(s) = \frac{R_3 \cdot (1 + s \cdot T_1)}{(R_1 + R_2 + R_3) \cdot (1 + s \cdot T_2)}, \tag{1.2}$$

where the time constants T_1 and T_2 are functions of the resistors and capactors. With this model the analysis of power consumption was performed for rectangular, sinusoidal and triangular input waveforms.

Bao et al. have modelled IPMC taking into account the effect of relaxation of the bending IPMC described by many authors [2, 4, 22, 23]. Under a step voltage, after a very quick bending towards the anode, the strip shows a slow relaxation towards the cathode. The model assumes that the positive ions bring more water to the cathode than there should be in the equilibrium. There is a diffusion of the water back to the anode after initial moving to the cathode and leakage of the water together with the ions out of the membrane through the cracked metal coating [24].

The model is a circuit, similar to the model of Jung, consisting of resistors and capacitors as depicted in Fig. 1.6. [24].

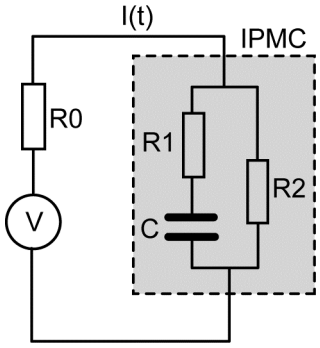

Figure 1.6. The model of Bao et al.

Under step input voltage the input current of the circuit is expressed as

$$I(t) = \frac{V}{R0 + R2} \cdot (1 + (\frac{R1 + R2}{R} - 1) \cdot e^{-\alpha \cdot t}), \tag{1.3}$$

where

$$R = R1 + \frac{R0 \cdot R2}{R0 + R2} \quad \text{and} \quad \alpha = \frac{1}{R \cdot C}. \tag{1.4}$$

The electromechanical response of the actuator is expressed as a function of electric current – the movement of the cations together with associated water molecules in the electric field.

$$\frac{dk}{dt} = K_1 \cdot \frac{dq}{dt} - \frac{1}{\tau} \cdot (k - K_2 \cdot q), \tag{1.5}$$

where q is an electrical parameter – electric charge and k is a geometrical parameter of the actuator – curvature. K_1, K_2 and τ can be found by curve-fitting the experimental data.

It is assumed that the model without relaxation is a special case of a model with relaxation, in the simplest case the curvature is proportional to the current:

$$\frac{dk}{dt} = K_1 \cdot \frac{dq}{dt} \quad \text{or} \quad \frac{dk}{dt} = K_1 \cdot I(t) \tag{1.6}$$

Bonomo et al. elaborate the model by adding a pair of antiparallel diodes to the circuit describing the nonlinearities of the input current absorbed by the actuator as presented in Fig. 1.7. [25]. The influence of the diodes appears only when the voltage on them exceeds some critical value. The diodes in the model are described by adapting the Shockley ideal diode equation.

The mechanical response of the actuator is induced by the current passing through the branches $R2-C2$ and $R3-C3$ reflecting the capacitive nature of IPMC. The coupling between the electrical parameters and deflection of the beam is realized similar to the linear model of Newbury described hereinabove. This model takes into consideration the viscoelastic properties of IPMC.

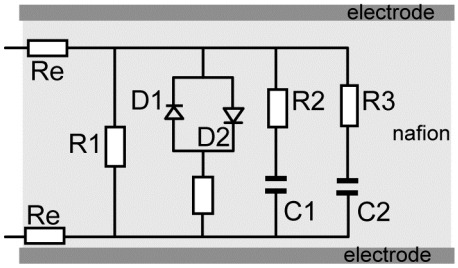

Figure 1.7. Bonomo's model.

About two years after their first model, Kanno et al. have proposed another, distributed model of an IPMC [26].

The actuator is divided into ten elements consisting of circuits similar to the models of Bao et al. or Jung, described above (Fig. 1.5, Fig. 1.6). The model of the IPMC shown in Fig. 1.8. consists of a series of connected resistors *Ra* and *Rb*, indicating the surface electrodes along the IPMC. Between the resistors representing the two surfaces there are single-unit cells consisting of resistors *Rx* representing the resistance of the polymer gel layer as an electric conductor and a capacitor *C* in conjunction with resistor *Rc* representing the characteristics of the exponential step response curve of the current. This combination forms a 2-dimensional linear approximate model of the IPMC.

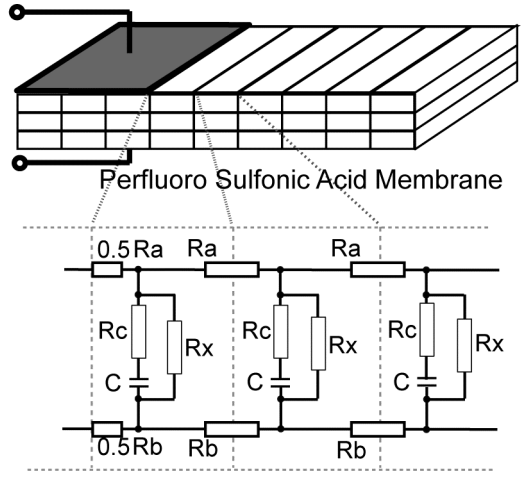

Figure 1.8. The Distributed model of Kanno et al.

The electromechanical coupling is divided into three stages:

1) Electrical stage: the electrical input current is derived from the input voltage pulse;
2) stress generation stage: time derivative of the current generates internal stress for bending with a 2-nd order delay;
3) mechanical stage: expansion and contraction of the surfaces induces bending motion of the actuator.

As a result, the current, stress generation function and the mechanical response are expressed by the equation, similar to that of a piezoelectric element.

$$\sigma = D(s) \cdot \varepsilon - K \cdot \left(\frac{\omega_n^2 \cdot s}{s^2 + 2 \cdot \varsigma \cdot \omega_n \cdot s + \omega_n^2}\right) \cdot I \ , \qquad (1.7)$$

where σ is an internal stress vector, ε is a strain vector and $D(s)$ is a mechanical characteristics including mass, dumping and stiffness. K is a transformation tensor of stress generation, ς and ω_n are the parameters of the 2-nd order delay, and I is current through the actuator [26].

Another similar distributed equivalent circuit is described by Shahinpoor [4, 27]. In this approach the units are connected in a series of resistors representing surface resistance. The circuit is presented in Fig. 1.9. There are four elements in each single unit: the resistance of the polymer; the capacitance representing the double layer at the surface-electrode/electrolyte interface and the electrode resistance Rss applied between the surface conductivity and other elements. The element Z is described as an unknown intricate impedance caused by charge transfers near the surface electrodes.

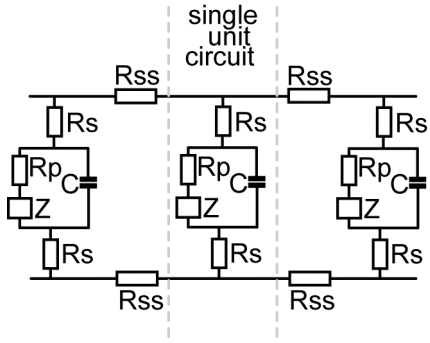

Figure 1.9. The Distributed model presented by Shahinpoor [27].

1.5. Fabrication of IPMCs

The fabrication of an IPMC involves two main stages: metallization of the surfaces of the polymer membrane and introduction of the ions into that membrane [2, 28].

The current state-of-the-art of the metallization technique of the membrane incorporates two distinct preparation processes: *initial compositing process* and *surface electroding process*. Due to the different preparation processes, morphologies of precipitated platinum are significantly different. The initial compositing process requires an appropriate platinum salt such as $Pt(NH_3)_4Cl_2$ for the chemical reduction processes. The principle of the compositing process is to metallize the inner surface of the material (usually, in a membrane shape, Pt nano-particles) using a chemical-reduction ingredient such as $LiBH_4$ or $NaBH_4$. The ion-exchange polymer is soaked in a salt solution to allow platinum-containing cations to diffuse *via* the ion-exchange process. After this process, a proper reducing agent such as $LiBH_4$ or $NaBH_4$ is introduced to platinize the materials by molecular plating. As a result, the metallic platinum particles are not homogeneously formed across the material but concentrate predominantly near the interface boundaries, as seen in the Fig. 1.10. It has been experimentally observed that the layer of the platinum particulates is buried a few micron deep (typically 1–10 μm) within the IPMC surface and is highly dispersed. The near boundary region of an IPMC strip on the penetrating edge of the IPMC shows a functional particle density gradient where the higher particle density is toward the surface electrode. The range of average particle sizes was found to be around 40–60 nm. The polymer-metal interface has critical influence on the IPMC performance; yet, the relationship is not well understood.

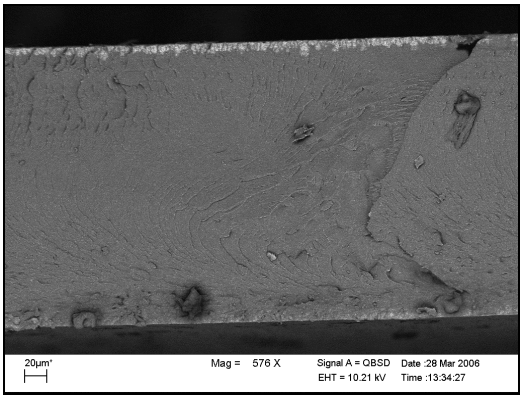

Figure 1.10. A SEM image of the cross-section of IPMC.
The surface electrode is easily identifiable.

During introduction of the cations into the polymer the proton connected to the chemical unit at the end of a side chain of the polymer is replaced with a cation. Usually it is done by soaking the membrane in a solution of salt or hydroxide of the corresponding cation.

Deciding on the basis of the research published in the last few years, the most frequently used ionomers are Nafion™ by DuPont and Flemion™ by Asahi Glass. The most commonly used materials for electrodes are platinum and gold. The commonly used cations are Li^+ and Na^+, as well as the larger organic cations tetraethylammonium (TEA^+) and tetrabutylammonium (TBA^+).

1.6. Possible applications of IPMCs

The high strains of IPMCs make them attractive as mechanical actuators for applications requiring large actuator displacement but little force. The low driving voltage and high current make them suitable for applications where high voltages are undesirable.

There exist a rapidly increasing number of studies where one or another of these properties is exploited for a great variety of applications. For example, IPMC sensors are investigated as vibration sensors for active noise damping [29, 30]. Even a larger amount of studies make use of the actuator properties of the IPMC materials. Their large actuation strain, displacement and flexibility make them suitable for artificial muscles in bio-inspired devices. During the last years many prototypes have been developed and reported.

A promising application area of IPMCs is biomedical assisting devices, for example artificial ventricular or cardiac-assist muscles, artificial sphincter and ocular muscles, surgical tools or peristaltic pumps [31]. Other applications using IPMC actuators include pumps and grippers [32, 33].

The natural mechanical response of IPMC is bending. Using a clever mechanical design, it is possible to convert the bending motion to a linear motion [34–37]. A mechanism for a walking robot is developed using linear IPMC actuators [34, 35].

There are several kinds of swimming fish-like microrobots utilizing IPMC actuators. A mechanism for underwater micro mobile robot has been investigated in [38, 39]. Several fish-like underwater robots are designed and implemented [40–45, **VII**, **VIII**].

Several authors describe IPMC manipulators, where the higher number of degrees of freedom is achieved by laser ablation of the metal coating. After metal plating a pattern is cut on both sides of the membrane. By patterning, the thin metal layer is removed and insulations between segments of the electrodes are achieved [46–48]. There have been attempts to couple laser patterned sensor and actuator segments on a single piece of a patterned polymer backbone [49, 50].

In spite of all efforts to create IPMC applications, the state-of-the-art is that all applications exist only as scientific projects or prototypes. There are no industrial applications or devices based on IPMC materials yet.

1.7. Research Goals and Contributions

The models published in the scientific literature to date almost universally describe IPMC actuators as a single piece with lumped parameters. For an actuator, the commonly used input parameters are electrical: voltage or electric current. The output parameters are the mechanical parameters of one particular point of the actuator, usually the tip – displacement of the tip or blocking force of the tip. For IPMC sensors, the commonly used parameters are the opposite – the input parameter is the deflection of the tip of a cantilevered strip of the IPMC; the output parameter is voltage or current produced by the device.

The contribution of my thesis with respect to the previous work is the following:

- The methodology of characterizing a bending cantilever beam IPMC actuator to measure the distributed mechanical and electrical properties of the IPMC. Using that methodology I have shown that the surface resistance of the metal electrodes is highly correlated to the bending curvature and improved the Kanno's model accordingly.
- Development of a distributed electromechanical model of IPMC sensors and actuators that describes the shape of the actuator in response to the electrical stimulus. Instead of describing the tip motion or motion of a particular point, the distributed model permits characterizing the continuous surface of an unevenly bending actuator. The model is based on RC transmission lines and unlike other models, takes into account the changing surface resistance of a bending actuator. It must be pointed out, that the model described in this work does not consider the static mechanical parameters of an IPMC, for example the viscoelasticity of the polymer membrane, the blocking force produced by the IPMC actuator, inertia, etc.
- The development of a self-sensing IPMC actuator. Apart from the sensors and coupled sensors and actuators developed and analyzed so far, the self-sensing actuator exploits the voltage drop on the surface resistance to measure the position and motion of the actuator.
- The development of an S-shaped actuator that exploits the phenomenon of a resistance increase in response to the increased curvature.

The rest of this thesis describes my contribution to electromechanical modeling of IPMC sensors and actuators. It is organized in a following manner.

First I describe the methodology that I have developed and that later on permitted me to describe the distribute parameters of the IPMC sensors and actuators. This methodology is described in Chapter 2.

Chapter 3 describes the distributed electromechanical model of an IPMC actuator, based on RC transmission lines.

Close inspections of the parameters of IPMC actuators revealed, that the resistance of the metal electrodes of IPMC is not constant. The surface resistance depends on the flexure of the particular piece in the particular area. The changing surface resistance affects significantly the behaviour of IPMC-based actuators and sensors. Description of the phenomenon of the varying surface resistance and the refined model is described in Chapter 4.

Chapter 5 describes the distributed electromechanical model of an IPMC sensor, based on RC transmission lines.

The distributed electromechanical model of an IPMC incorporates several electrical parameters. A possible methodology of identification of the parameters is presented in Chapter 6.

Chapter 7 describes, how the nonlinearities caused by electrochemical electrode reactions affect the distributed electromechanical model of an IPMC actuator.

The effect of the varying resistance of the electrodes of the IPMC is exploited in the principle of a self-sensing IPMC actuator described in Chapter 8.

Due to the increasing resistance of the bending electrodes the actuator may have more than a single pair of feeding contacts. A S-shape actuator is described in Chapter 9.

1.8. Technical Notes

If not noted otherwise, all experiments and measurements described in the current work and the published papers have been conducted using the IPMC material – Musclesheet™, provided by BioMimetics Inc. in 2004. Musclesheet™ consists of a 0.2…0.5 mm thick proprietary ionomer, similar to Nafion, covered with platinum electrodes. The ions introduced to the ionomer were Na^+ or Li^+.

Musclesheet™ is a water-containing IPMC, intended to work in a wet environment. If not noted otherwise, in the course of the experiments the pieces of Musclesheet™ have been completely submerged in a container of deionized water.

2. ELECTROMECHANICAL CHARACTERIZATION OF IPMCs

This chapter describes the methodology of measuring the electrical and mechanical characteristics of a bending IPMC cantilever actuator. The distributed electromechanical model is developed based on these experimental results and also validated using this methodology. It describes how the electrical parameters are measured and presented, how the mechanical parameters of the bending actuator are obtained and how these results are later combined together.

2.1. Characterization of electrical parameters

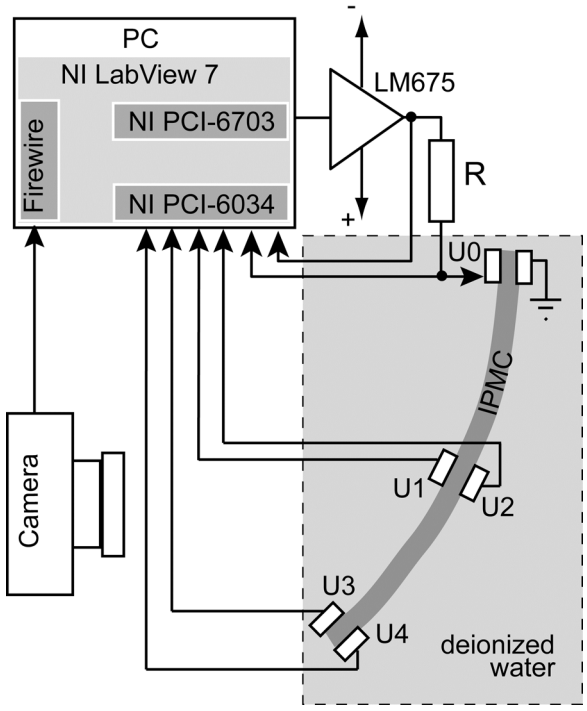

Figure 2.1.1. Experimental setup.

The experimental setup is shown in Fig. 2.1.1. The actuator is clamped in a vertical cantilever position in a container filled with deionized water. The input voltage is applied to the actuator via a fixed contact pair $U0$ and a ground contact. At the free end of the actuator an additional pair of contacts $U3 - U4$ is attached. Optionally at the middle of the actuator a pair of contacts $U1 - U2$ may be attached. These contacts together with their clamps should be as

lightweight as possible in order to prevent any mechanical disturbance. Some examples of the clamps are presented in Fig. 2.1.2.

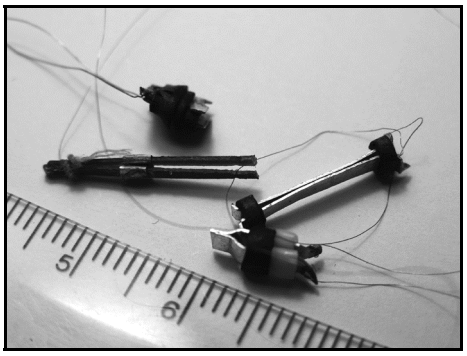

Figure 2.1.2. Some examples of the clamps.

The wires connected to the contacts $U1$ – $U4$ and the measuring system should be thin (~ 0.08 mm) to prevent them from disturbing the actuator. As the measured parameter is voltage, the electric current in the wires is negligible and there will be no voltage drop in the wires.

The electric input current is measured as a voltage drop over the resistor R. The value of the resistor should be chosen as low as possible, but still sufficiently high with respect to the value of the current and the sensitivity of the measuring equipment. In the course of the experiments described in the current work, the value of the resistor R was 0.05…1Ω.

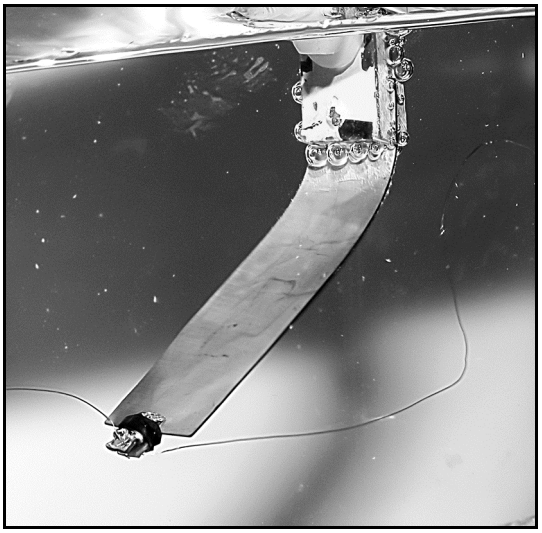

Figure 2.1.3. A cantilever IPMC actuator with one pair of additional contacts.

The measurements were conducted with National Instruments LabView7 control software. Due to the features of the equipment, the measurements were performed using a “common ground” circuit, i.e. all voltages were measured

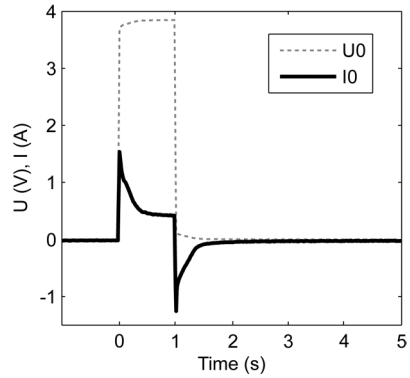

Figure 2.1.4. Input voltage U0 and input electric current I0.

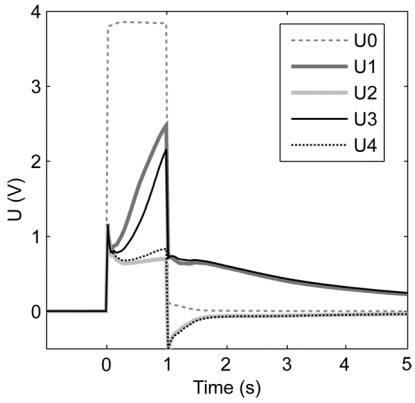

Figure 2.1.5. Voltage drops along the electrodes.

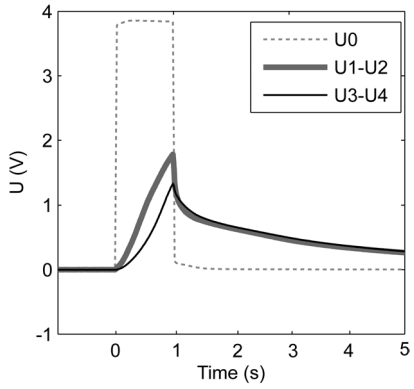

Figure 2.1.6. Voltages between the electrodes.

with respect to the ground and one input contact of the IPMC sample was also connected to the ground. The driving voltage was generated by NI PCI-6703 DAQ board and amplified with NS LM675 power op-amp. Voltages on all contacts with respect to the ground were measured with National Instruments PCI-6034 DAQ board. This setup makes it possible to measure the response voltage drops along the surfaces of the device in the time domain. The voltage between the contacts is calculated as a difference of the two signals.

Fig. 2.1.4–2.1.6 depict the typical recorded signals. The voltages between the contacts at the free tip of the actuator (Fig. 2.1.6) increase and decrease roughly exponentially while the demeanour of the voltage drop along the actuator, Fig. 2.1.5 performs a specific turn in the beginning of the input pulse.

If the contact clamps are sufficiently lightweight and the actuator is strong enough, attaching more contact pairs to the device allows monitoring the behaviour of the voltages along the device in detail. The experiments given in **IV** are conducted using 3 pairs of contacts.

The experiments exhibit, that the voltage along the surface is not uniform, but grows and propagates slowly similar to a charging and discharging capacitor. This is caused by the capacitive nature of the IPMC and the non-zero surface resistance. In case of a rectangular input voltage pulse the voltage grows faster at the input contacts and more slowly at the free end of the actuator. After disengaging, the voltage decays faster at the input contacts and slower further away from the contacts. As the result the actuator performs a sharp bending motion. The voltage between the sides of the tip equals to the input voltage only in case of sufficiently long-lasting input voltage.

The voltage between the sides of the tip of the device depends on the conductance of the surface electrodes and the electrochemical pseudo-capacitance of the particular piece of the material.

2.2. Characterization of the shape of the actuator

As explained above, generally the models of an IPMC described in the scientific literature do not characterize the shape of IPMC-based devices. These models usually describe the motion of the tip or the blocking force of the tip of the device. The equipment used to characterize the parameters are for instance laser position sensors or force gauges [21, 29, 51, 52, 53].

In order to describe the mechanical motion of the actuator, a simple computer vision system was developed. It consists of a fast CCD camera and a PC with image processing software. The National Instruments Vision was used for both frame grabbing and image processing.

The bending motions of the actuator are recorded with the camera. I used a high-speed firewire camera *Dragonfly Express* from *Point Grey Research Inc.* This camera is capable of recording images at the speed up to 200 frames per

second. The direction of the camera is set transverse to the actuator and the experiment is illuminated from the background through a frosted glass. In perfect conditions the image of the actuator recorded in such a way consists of a single curved contrast line as depicted in Fig. 2.2.1. It is easy to use image processing software to process the shape of the actuator during each particular frame.

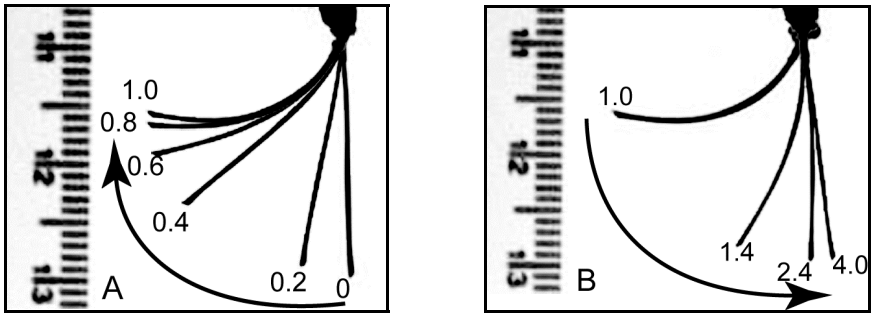

Figure 2.2.1. A series of frames showing the response of an actuator to a 1s driving voltage pulse.
A – actuation during the pulse; B – relaxation after the pulse.
The numeric characters indicate the time instant of the frame.

It is apparent in Fig. 2.2.1, that in the beginning of the input pulse (images 0...0.4s in Fig. 2.2.1.-A) the actuator performs a sharp motion close to the input contacts only, the free end remains almost straight. Later (images 0.4...1.0s in the Fig. 2.2.1.-A) the flexure of the actuator propagates gradually on, but the flexure at the region close to the contacts does not increase any more. During the relaxation (images 1.0...4.0s in the Fig. 2.2.1.-B) the sharp decrease of the flexure takes place close to the input contacts again, whereas the remaining part of the actuator straightens slowly in few seconds.

We describe the motion of an actuator as follows. The image processing software divides the image of the actuator into vectors with equal lengths as shown in Fig. 2.2.2. For each vector the angle with respect to the direction of the previous vector a_i is registered. The matrix of changing angles a_1 ... a_n describes the bending motion of the actuator. This method of describing the shape of the actuator allows representing its mechanical bending motion in the time domain as a series of 2D graphs or, more illustratively, as a 3D surface.

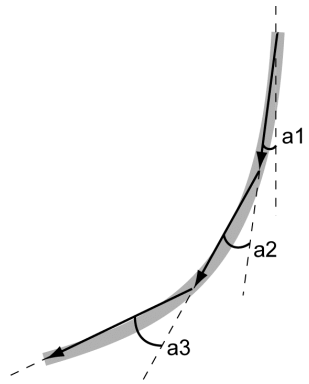

Figure 2.2.2. Characterization of the flexure.

Fig. 2.2.3. shows the 3D graph characterizing the changing flexure of the actuator shown in Fig. 2.2.1. It can be observed that the bending of the sheet is faster and stronger close to the input contacts, getting progressively weaker as well as delayed towards the free end of the sheet.

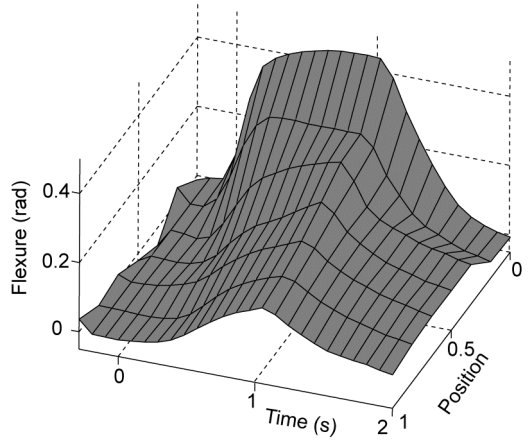

Figure 2.2.3. Mechanical response of an actuator to step input voltage. The "Position" axis stands for the relative coordinate starting from the input contacts.

The actual number of vectors depends on the optical resolution of the camera. Using the lense Pentax C-3516M with the focal length of 35mm, we were able to divide the image of the up to 40 mm long IPMC strip into 5…12 vectors. In Fig. 2.2.3. the number of vectors was 7.

2.3. The combination of electrical parameters and shape

The CCD cameras are usually capable of recording images only at some fixed relatively low frame rates. The equipment for electrical measurements is capable of measuring the voltages and record the results at a very high speed. It is not necessary to attempt to synchronize the two processes. Scaling the two graphs to a common timescale and positioning one above the other gives an opportunity to compare the electrical and mechanical parameters. It turns out that the two graphs – the graph of spreading voltages along the surface and the graph of bending angles along the surface are strikingly similar, as presented in Fig. 2.3.1. and **IV.**

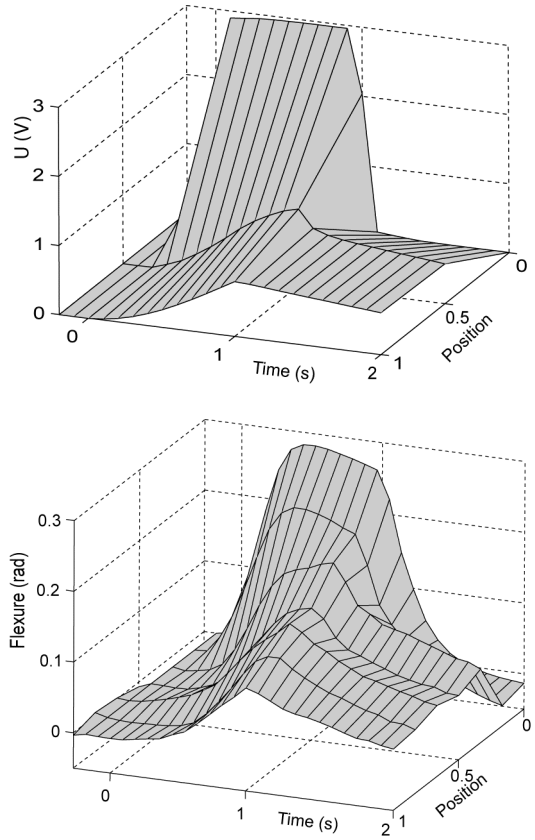

Figure 2.3.1. The comparison of the graph of the spreading voltages along the surface and the graph of the bending angles along the surface.

3. A DISTRIBUTED MODEL OF IPMCs

The fact that the electrical perturbation as well as the change of the flexure spread along the actuator at finite speed; and the described similarity between the two graphs were the motivations to develop a distributed model of an IPMC.

The basis of the model is the distributed model of an IPMC proposed by Kanno et al. in 1996 described afore. [26]. Originally Kanno divided a piece of an IPMC into ten similar segments and modelled the relation between the input current and tip displacement. Dividing the same piece into an infinite number of infinitesimally short similar segments, gives an RC transmission line. Actually, the elaborated model of Kanno models an IPMC as a leaky distributed thin-film capacitor with poor electrode conductivity and considerable shunt losses. In fact, the circuit represents a lossy RC-transmission line.

There are two fundamental causes of the electric current between the electrodes of an IPMC through the polymer matrix:

1. The current caused by ionic conductivity. Relocating ions constitute the pseudocapacitance of the double-layer which forms at the interface between the ion exchange membrane and the metal electrode [7]. As described hereinabove, the resulting irregular density of hydratized ions is the cause of bending of the IPMC. The resulting deformation of the IPMC is proportional to the total amount of relocated ions. In the equivalent circuit the pseudocapacitance is depicted as shunt capacitors between the electrodes in each single unit.
2. The current caused by electrochemical electrode reactions, for example electrolysis of the solvent. The electrode reactions appear only if the voltage between the electrodes exceeds some certain critical level, depending on the materials used. The presence of the electrode reactions wastes energy and affects the propagation of voltage, but does not have direct effect on the deformation of the IPMC. In the equivalent circuit the electrode reactions are depicted as shunt resistors between the electrodes in each single unit.

If the voltage between the electrodes of an IPMC is lower than the voltage required for the electrolysis of the solvent, the influence of electrochemical electrode reactions can be neglected. The current passing through the polymer matrix is caused solely by ionic conductivity. The simplified model is presented in Fig. 3.1. The resistances of both electrodes in each single unit are depicted as resistors Ra and Rb; the pseudocapacitance is depicted as capacitor C.

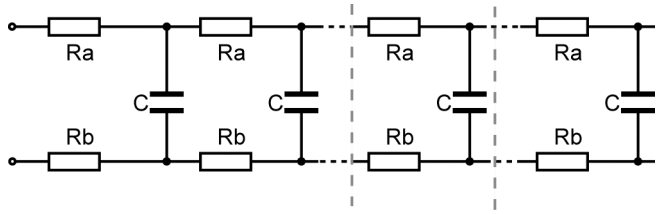

Figure 3.1. The equivalent circuit of an IPMC.

The voltage and current along the resulting uniform RC transmission line can be described after transforming it to a Cauer equivalent ladder structure [54], as presented in Fig. 3.2.

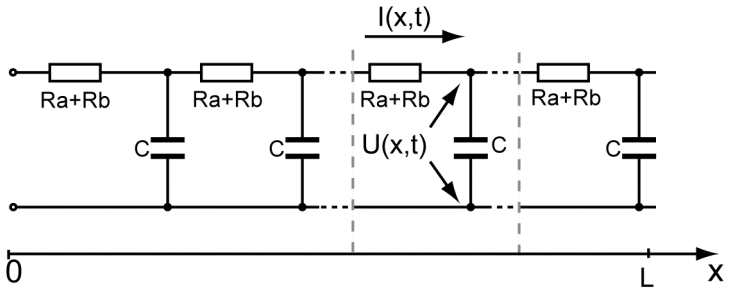

Figure 3.2. The Cauer ladder structure of the equivalent circuit.

A comprehensive overview of the lossless uniform distributed transmission line in the time domain considering different bounder conditions is presented in [54, 55].

The pair of linear differential equations which describe the voltage and current on an electrical transmission line with distance and time are called the telegrapher's equations (or just telegraph equations). The equations come from Oliver Heaviside who developed the transmission line model [56]. The theory applies to high-frequency transmission lines (such as telegraph wires and radio frequency conductors) but is also important when designing energy transmission lines. The model demonstrates that the electric current can be reflected on the line, and that wave patterns can appear along the line.

Using the notations given in Fig. 3.2., and converting the resistances and capacitances to the values per unit length, the following relations can be given between the currents and voltages:

$$\frac{\partial U(x,t)}{\partial x} = -(ra + rb) \cdot I(x,t) \tag{3.1}$$

$$\frac{\partial I(x,t)}{\partial x} = -c \cdot \frac{\partial U(x,t)}{\partial t}, \tag{3.2}$$

where ra, rb and c are the resistances of the both electrodes and capacitance of the line per unit length respectively.

Substituting the equation (3.1) after derivation into the equation (3.2) results in

$$\frac{\partial U(x,t)}{\partial t} = \frac{1}{(ra+rb)\cdot c} \cdot \frac{\partial^2 U(x,t)}{\partial x^2} . \tag{3.3}$$

This shows that the time-dependent voltage along the line $U(x,t)$ is determined by a homogeneous, constant-coefficient, second-order partial differential equation, with the first time derivative on one side and the second spatial derivative on the other side. This kind of equation is called a diffusion equation, as diffusion processes are described using such equations. The general solution of voltage is a function of distance x and time t:

$$U(x,t) = (K_1 \cdot \sin(u \cdot x) + K_2 \cdot \cos(u \cdot x)) \cdot K_3 \cdot e^{-\frac{u^2}{(ra+rb)\cdot c}\cdot t} , \tag{3.4}$$

where u, K_1, K_2, and K_3 are constants and ra, rb and c are the resistances of the both electrodes and capacitance of the line per unit length respectively.

Mostly the differential equations are not solvable in a closed form. The step response of a uniform initially discharged RC transmission line is an exception. The step input voltage is also easily applicable to IPMC actuators.

An IPMC actuator can be described as an open-ended transmission line having finite length L. The voltage along an open-terminated finite-length uniform RC transmission line under step-voltage excitation is solvable in a closed form and is given by the following formula:

$$U(x,t) = \sum_{n=0}^{\infty} ((-1)^n \cdot (erfc((2n+\frac{x}{L})\cdot\sqrt{\frac{(Ra+Rb)\cdot C}{4t}}) + \\ + erfc((2n+2-\frac{x}{L})\cdot\sqrt{\frac{(Ra+Rb)\cdot C}{4t}}))) \tag{3.5}$$

[54, 55]. Here Ra, Rb and C are the total resistance and capacitance of the transmission line with the length L, and $erfc(x)$ is the complementary error function.

This equation converges fast and only few first terms are sufficient to get a good accuracy for short time intervals. The actual number of terms depends on the actual values of the parameters and the desired accuracy, and should be calculated for each particular case.

As described hereinabove, the deformation of an IPMC actuator is caused by the relocated ions, or by the current through the capacitors C in the distributed model. The electric current through an infinitesimally short segment dx of the transmission line is defined by the capacitance of the segment $C \cdot dx$ and the derivative of the voltage with respect to time:

$$dI(x,t) = C \cdot dx \cdot \frac{dU(x,t)}{dt}. \tag{3.6}$$

In case of a step-voltage excitation of an open-ended transmission line having a finite length L, where the voltage along the line is described with the equation (3.5), the electric current through the line at the position x and time t is also solvable in a closed form:

$$\frac{dI(x,t)}{dx} = C \cdot \sum_{n=0}^{\infty} \left(\frac{(-1)^n}{2t\sqrt{\pi}} \sqrt{\frac{(Ra+Rb)\cdot C}{t}} \cdot \right.$$
$$\cdot \left(2n + \frac{x}{L}\right) \cdot e^{-\frac{1}{4}\cdot\left(2n+\frac{x}{L}\right)\cdot\frac{(Ra+Rb)\cdot C}{t}} \cdot$$
$$\left. \cdot \left(2n + 2 - \frac{x}{L}\right) \cdot e^{-\frac{1}{4}\cdot\left(2n+2-\frac{x}{L}\right)\cdot\frac{(Ra+Rb)\cdot C}{t}} \right) \tag{3.7}$$

For the purpose of coupling the electrical and mechanical models we assume that the degree of expansion of one side of an IPMC strip and the contraction of the opposite side $k(x,t)$ at a given point of the sample depend on the amount of the moved electric charges $q(x,t)$, possibly carrying water molecules at that point. The mechanical deformation and the electrical parameters can be coupled using the equation (1.5) from the model of an IPMC proposed by Bao et al. [24] described hereinabove. Assuming that there is no relaxation of an IPMC caused by water leakage, i.e. all moved charges produce deformation of the actuator, the dependency between the flexure and the amount of moved electric charges at that point is linear:

$$\frac{d}{dt}k(x,t) = K \cdot \frac{d}{dt}q(x,t) = K \cdot I(x,t). \tag{3.8}$$

In that case the total flexure at the given point x at time instance t can be calculated by summarizing all motions generated by all charges before the instant t:

$$k(x,t) = K \cdot \int_0^t I(x,t)dt. \tag{3.9}$$

Calculating $I(x,t)$ from (3.7) and deformation from (3.9) permits coupling the transmission line model of the IPMC to the mechanical bending. The equation (3.9) enables finding the flexure of the actuator at any point x at any time instance t and thus finding the shape of the IPMC actuator for non-uniform bending.

The distributed model of an IPMC is given in Fig. 3.3. Each single unit of the RC transmission line contains an ammeter measuring current I_C through the capacitance C. Current I_C is integrated with respect to time, resulting to the mechanical response *k* of the single unit.

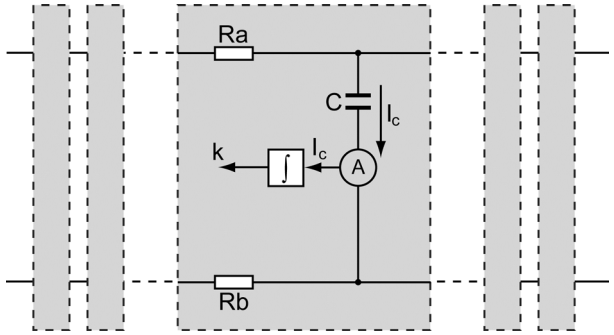

Figure 3.3. The distributed model of IPMC.

Some simulations of a step response of the actuators with various electrode resistance and capacitance values on similar scales are given in Fig. 3.4. – Fig. 3.7. The simulations are performed using equations (3.5), (3.7), (3.9). The values of the resistance and capacitance are close to the experimentally gained real values. As the coefficient K of the equation (3.9) is not determined yet and can be found by curve fitting, I do not give the scale of the vertical axis but only demonstrate the shape of the characteristics. There is an obvious similarity between the charts of voltage and the bending motion. Since current is a derivative of voltage and the flexure, in turn, is the integral of current, both with respect to time, the similarity is easy to explain.

In Simulation 1 the resistance of the electrodes, capacitance and length of the actuator are close to the experimentally measured values of the actuator described in paragraphs 2.1 and 2.2.

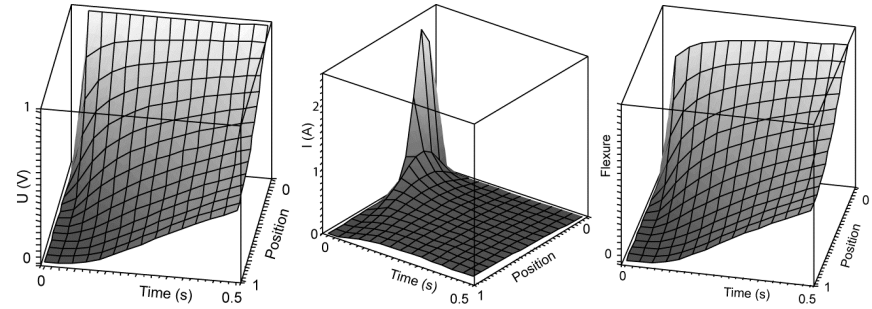

Figure 3.4. Simulation 1. C =0.1F; $Ra + Rb$ =15Ω.
A – voltage, B – current, C – flexion.

The voltage increases rapidly close to the input contacts and more slowly further away from the input contacts. The electric current peaks sharply near the input contacts during the first few milliseconds of the input pulse, and then decreases rapidly to almost zero towards the free end of the sample. This behavior of current produces a sharp bending close to the input contacts only. The noticeably weaker change of the flexure of the free end appears after a short delay. The behavior of voltage corresponds to the graph given in paragraph 2.1, Fig 2.1.4. – Fig. 2.1.6., and the change of flexure corresponds to Fig. 2.2.3.

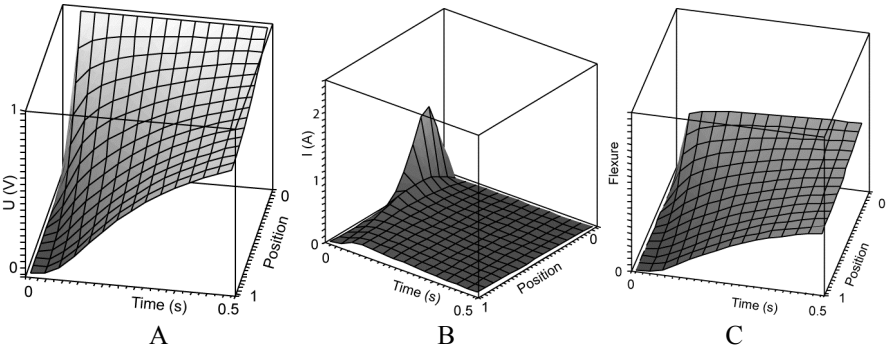

Figure 3.5. Simulation 2. C =0.05F; $Ra + Rb$ =15Ω.
A – voltage, B – current, C – flexion.

In Simulation 2 the capacitance of the actuator is twice less than in Simulation 1. When compared with the motion of Simulation 1, the motion of Simulation 2 is about twice weaker. This corresponds to the conclusion of Akle, that the strain response of an ionomeric transducer is strongly correlated to the capacitance of the plated material. Akle demonstrates that there is an approximately linear relationship between strain response per unit voltage and the capacitance of the transducer [57].

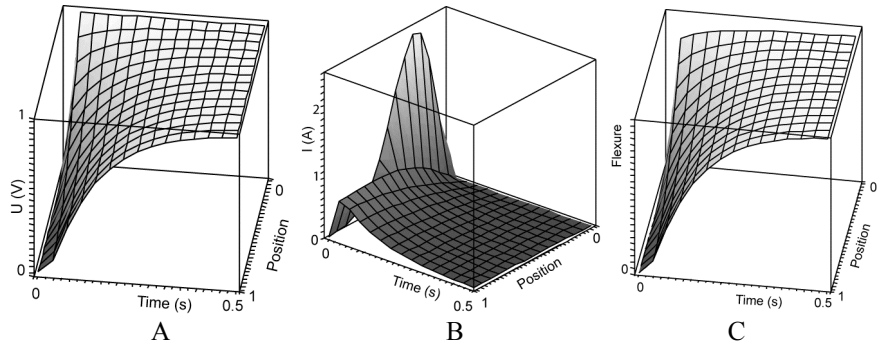

Figure 3.6. Simulation 3. C=0.1F; $Ra + Rb$=3Ω.
A – voltage, B – current, C – flexion.

In Simulation 3 the capacitance of the actuator is equal to that of Simulation 1, but the conductivity of the electrodes is 5 times higher. Although the free end of the actuator retards, due to the good conductivity there is no considerable voltage drop along the surface of the actuator and after half of a second already the flexure of the actuator becomes uniform, i.e. forming an arc of a circle. This conclusion is consistent with the observation given in [27] that the lower surface-electrode resistance generates higher actuation capability in the IPMC artificial muscles.

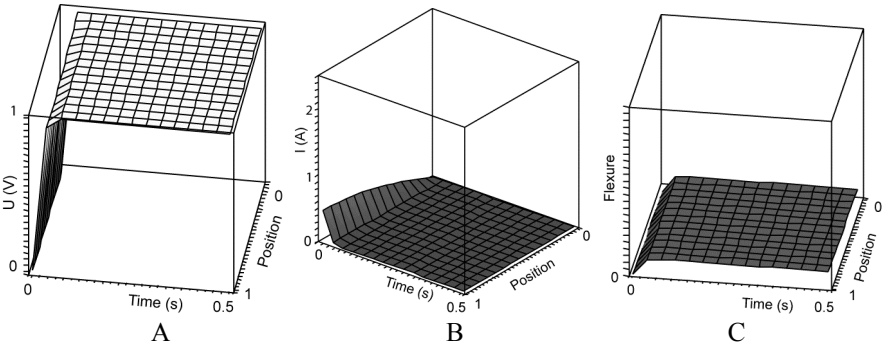

Fig. 3.7. Simulation 4. C=0.01F; $Ra + Rb$=3Ω.
A – voltage, B – current, C – flexion.

In Simulation 4 the conductivity of electrodes is high, but the capacitance is 10 times lower than in Simulation 1. The capacitance is low and the actuation capabilities are low due to deficiency of charged particles. Although the flexure of the actuator is low, it is continuously uniform, and achieves the maximum in about 20 milliseconds only.

The relationship between the actuation capabilities and length of an actuator is given in **III.** These simulations result to a conclusion that due to distributed capacitance and electrode resistance it is useless to have too long IPMC actuators. The optimal length of an actuator is actually a function of the product of the electrode resistance and pseudocapacitance of the particular IPMC material. If the material has better conductivity, i.e. resistance is lower and has better expected performance, then the optimal length is longer. If it has lower capacitance, i.e. contains less ions and therefore has weaker expected performance, the optimal length is also longer.

Anton et al. investigate the mechanical properties of an IPMC and the forces applied by IPMC actuators [58, 59]. Anton concludes that an IPMC actuator has finite optimal length depending on the particular task due to the uneven stress distribution even if the electrical parameters were homogeneous [59]. Presumably the consideration of the electrical as well as mechanical parameters gives a good approximation to the problem of the optimal length of an IPMC.

Although the analytical model shows a good correlation to the experimental data, the model only considers the case where an actuator containing water is driven at low voltages. At higher input voltages the electrode reactions cause considerable non-linearities. For the actuators where ionic liquid is used as a solvent, the linear model is expected to hold even at moderately large deformations and higher input voltages.

4. A NONLINEAR DISTRIBUTED MODEL

4.1. A characterization of surface resistance of IPMCs

The metal surface of the IPMC usually appears cracked, consisting of discrete particles [2, 27]. Supposedly these cracks are caused by water swelling and electroactive bending. Regardless of fractionation surface conductivity is large enough, as conduction occurs via contact of individual metal islands at the surface of the membrane [2].

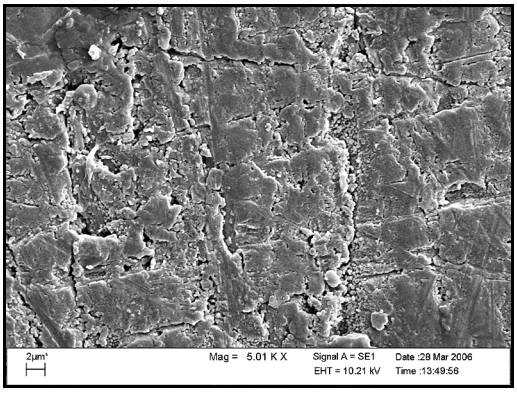

Figure 4.1.1. The surface of the IPMC is cracked.

During bending one face of the IPMC shrinks, the opposite face stretches swollen with water and ions. The natural cracks of the metal of the metallized surfaces shrink and expand causing surface resistance changes.

The measurements of the surface resistance revealed that when the surface of the IPMC is compressed, its resistance decreases slightly with the decreasing bending radius. When the sample is stretched, the resistance increases several times when the bending radius decreases. It is typical that the actual values of the surface resistance and the change are not equal on both sides. The change of the surface resistance of the stretching side is always larger than the change of the resistance of the compressing surface and we suggest that it depends on how the metal particles on the surface electrode are thorn apart or stretched out on the surface.

The first measurements were conducted bending the samples of an IPMC along the surface of round lab glassware with various diameters. A contact strip with 4 electrodes was fixed on the IPMC. In order to measure the expanding side of the IPMC strips they were attached to the outer surface of the glasses. To measure the compressed surface, they were attached to the inner surface.

Later an automatic device capable to change the flexion of an IPMC strip and measure the resistance of IPMC electrodes was built [60]. The device

employs two servos and one stepper motor to bend the sample of the IPMC as an uniform arc of a circle. The resistances of both surfaces of the sample are measured using four-probe method. The results of the measurements are sent to a PC using USB interface.

A typical result of the measurements is shown in Fig. 4.2. The origin of the horizontal axis denotes a loose sample. Along the positive direction of the horizontal axis the surface is progressively expanded; along the negative direction the surface is progressively compressed.

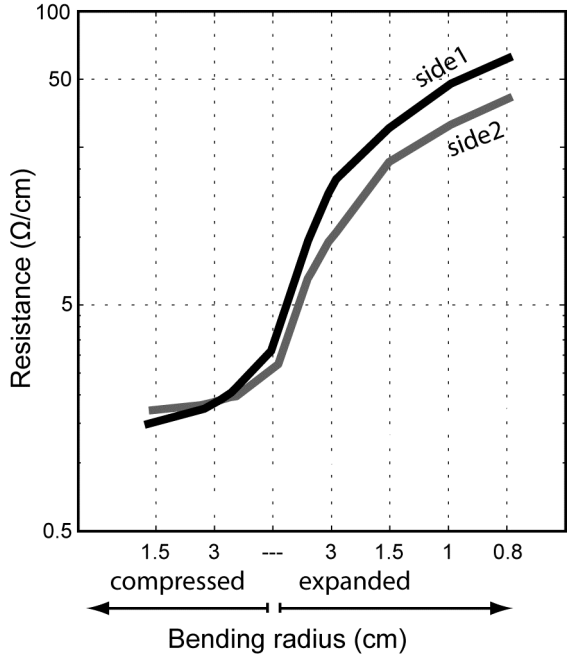

Figure 4.1.2. The correlation between the surface resistance and the bending radius of an IPMC sample.

The results suggest that the densely packed particles on the surface cannot be compressed any more, but can easily be drawn apart from each other when the top layer of the film is stretched. The surface resistance thus seems to depend on the contact area of the particles.

A comprehensive overview of the changing surface resistance and some experiments are provided in **I**.

4.2. A nonlinear equivalent electric circuit

The equivalent electric circuit of an IPMC, modelling the changing resistance of the electrodes is described in Fig. 4.2.1. Each single unit of the RC transmission line contains an ammeter measuring current I_C through the capacitance C. Current I_C is integrated with respect to time, resulting to the flexure *k* of the single unit according to the equation (3.9) derived from [24]. The improvement with respect to the model of Kanno [26] is that the resistors indicating the surface resistance of the IPMC *Ra* and *Rb* are variable resistors instead of constant-value resistors. The values of the variable resistors depend on the flexure *k* of the IPMC strip at the single unit according to the functions f_1 and f_2. When the surface stretches, the resistances of the variable resistors increase, when the surface compresses, the resistances decrease.

The resulting RC transmission line is a non-uniform transmission line at each time instance. A comprehensive theory of that kind of lines is given by E. Protonotarios et al. in [61, 62, 63]. According to [62] the voltage response of a non-uniform distributed RC transmission line to a unit-step excitation is a totally positive density function that possesses only one maximum. It behaves asymptotically for $t \to 0+$ and for $t \to \infty$. The voltage impulse response at any interior point of such line is a positive one-sided density function for $t > 0$.

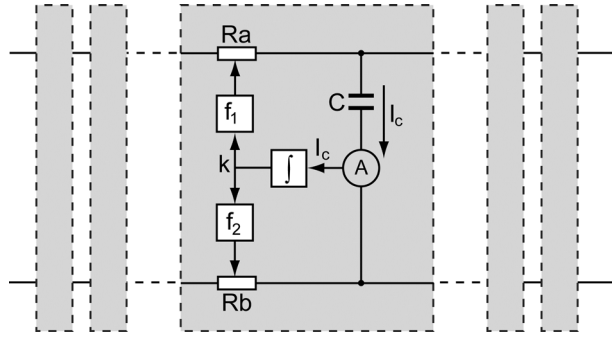

Figure 4.2.1. The equivalent circuit of an IPMC considering the changing resistance of the electrodes.

For the changing flexure, and hence for the changing resistances of Ra and Rb, the circuit forms a time-dependent non-uniform transmission line.

It must be pointed out that the closed-form solutions for the time-domain impulse response of non-uniform RC transmission line are practically impossible, and exact series expansions are possible only in rare circumstances. [54, 62, 64]. Some possible approximations of the solution are described for example in [64, 65]. The simplest method of solving the line is replacing the RC

transmission line by a lumped RC ladder. The distributed line can be approximated by a lumped RC ladder very simply. The disadvantage is that for a fair approximation a larger number of lumped elements must be used. The approximation is valid only in the low frequency region as the order of the network is zero [64].

4.3. Simulating the nonlinear actuator

For simulations of the equivalent electric circuit a Matlab Simulink model using the SimPowerSystems toolbox was created. It consists of 10 similar single units depicted in Fig. 4.2.1. The functions f_1 and f_2 are simulated according to the graphs side1 and side2 in Fig. 4.1.2. The comparative simulations expound in Figs. 4.3.1 – 4.3.5., are conducted according to the measurements given hereinabove in Chapter 2. The graphs A depict the case where the resistance of the electrodes is invariable; the graphs B are the results of the simulations where the resistance of the electrodes changes according to Fig. 4.1.2.

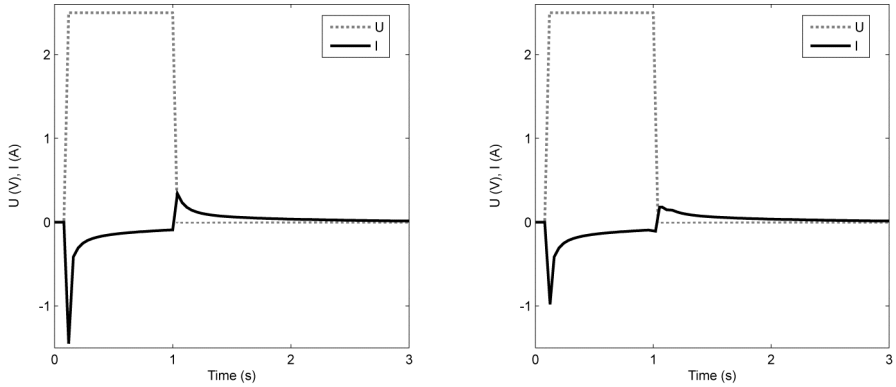

Figure 4.3.1. Input voltage and input electric current.
A – invariable resistance of the electrodes;
B – variable resistance of the electrodes.

In the beginning of the rectangular input voltage pulse the input electric current peaks sharply. When the input pulse terminates, the current performs a sharp peak with the opposite polarity. The graph corresponding to the measurement is depicted in Fig. 2.1.4. There is no noticeable difference between the two graphs of the different models.

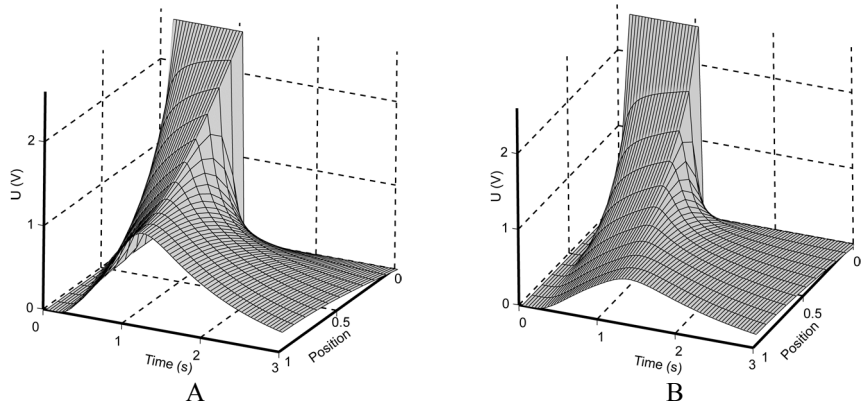

Figure 4.3.2. Distribution of voltage between the electrodes.
A – invariable resistance of the electrodes;
B – variable resistance of the electrodes.

The rectangular input voltage pulse decays fast. The amplitude of the voltage is considerable only in about one third of the length of the actuator. The amplitude of the voltage in the middle of the actuator is almost equal to the voltage at the free end. Similar behaviour of voltages are presented in Fig. 2.1.6. As the total resistance of both electrodes $Ra + Rb$ increases, the graph B is lower.

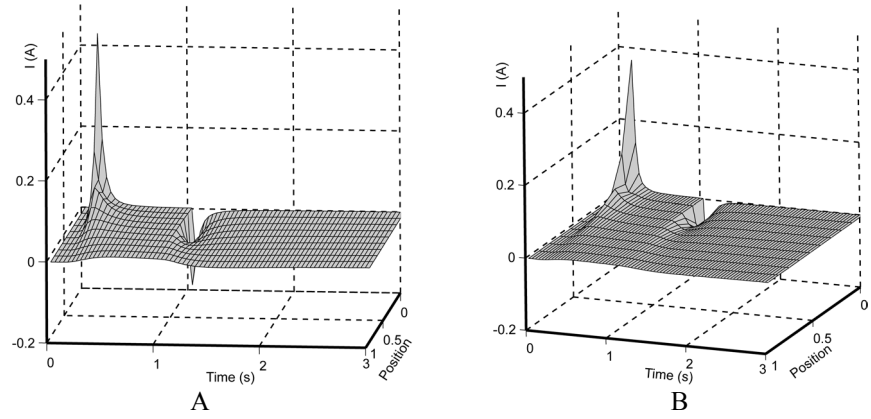

Figure 4.3.3. Distribution of electric current.
A – invariable resistance of the electrodes;
B – variable resistance of the electrodes.

The distribution of electric current through the polymer is a parameter, not measurable in the real systems. It can only be simulated. Near the input contacts the electric current peaks sharply and decays rapidly. Further away from the input contacts the current increases smoothly. The graph B is lower, but the

detailed difference between the graphs A and B is visible only at a close examination.

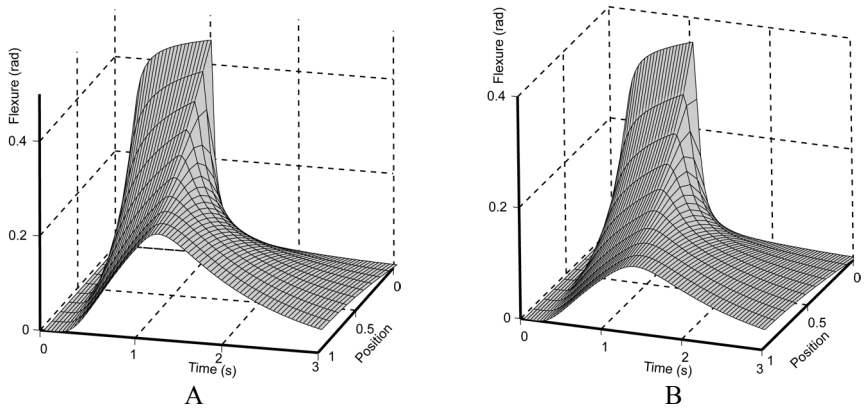

Figure 4.3.4. Bending motion.
A – invariable resistance of the electrodes;
B – variable resistance of the electrodes.

The change of the flexure of the actuator is achieved by integrating the electric current with respect to time according to (3.9). The similar change of the flexure is depicted in Fig. 2.2.3 and Fig. 2.3.1., obtained from the measurements with real actuators. In order to obtain the amplitude of the flexure similar to Fig. 2.3.1., the coefficient K of the equation (3.9) is approximately 40. As the total resistance of both electrodes $Ra + Rb$ increases, the graph B is lower.

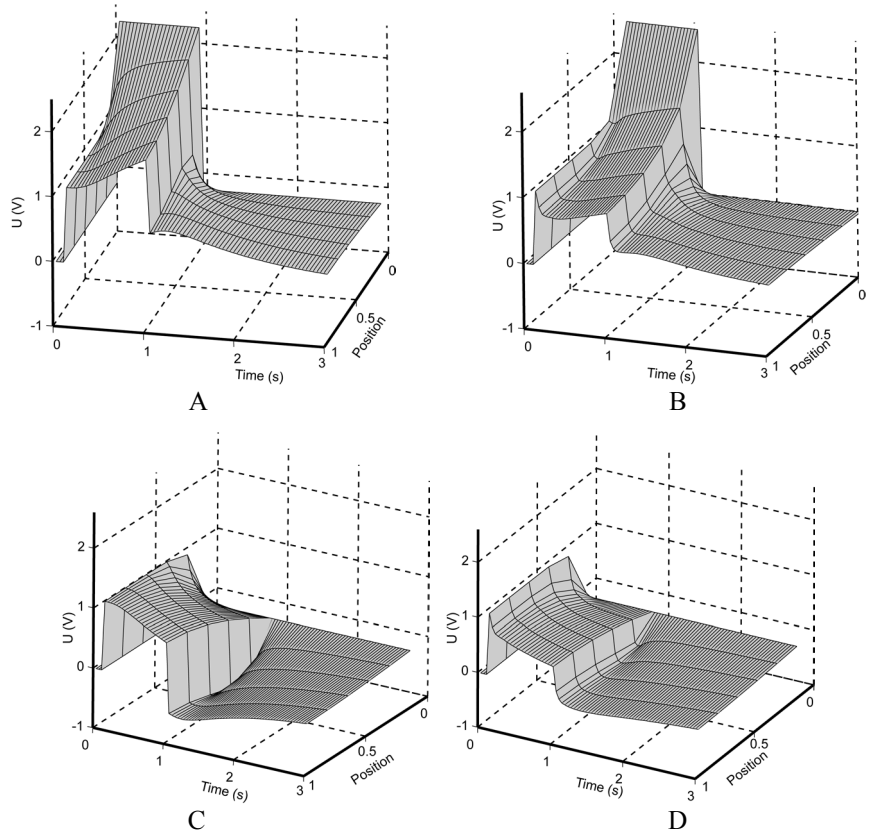

Figure 4.3.5. Voltage drops along the length of the actuator on both sides.
A – side 1, invariable resistance of the electrodes;
B – side 1, variable resistance of the electrodes;
C – side 2, invariable resistance of the electrodes;
D – side 2, variable resistance of the electrodes.

The graphs presented in Fig. 4.3.5. correspond to the measured voltages shown in Fig. 2.1.5. The voltages between the sides of the actuator (Fig. 4.3.2) are rather similar in cases of both changing and constant resistances of the electrodes. The voltage drop along the length of the actuator performs a specific turn in the beginning of the motion, caused by the increasing total resistance of both electrodes $Ra + Rb$. Similar specific turn is identifiable in the measurement depicted in Fig. 2.1.5.

This characteristic behaviour of the voltage drops along the electrodes can be utilized to identify the bending of an actuator, as described hereinafter.

5. A DISTRIBUTED MODEL OF THE IPMC SENSOR

Mechanical bending of the IPMC material contracts one side of the membrane while expands the other. This forces the mobile ions, carrying the water molecules, to move against the pressure gradient. The expanded side therefore contains an excess of positive ions. This phenomenon produces a voltage gradient at the surface electrodes of the IPMC [2, 16, 27].

The forced flux of ions can be introduced into the distributed model of IPMC as a distributed source of electric current. Besides the already introduces variable resistors *Ra* and *Rb* and a capacitor C, each single unit of the RC transmission line depicted in Fig. 5.1. contains a generator of electric current J. The change of flexure k of each single segment $\frac{\partial k(x,t)}{\partial t}$ and the current $I_k(x,t)$ generated by the generator of current J have a functional relationship.

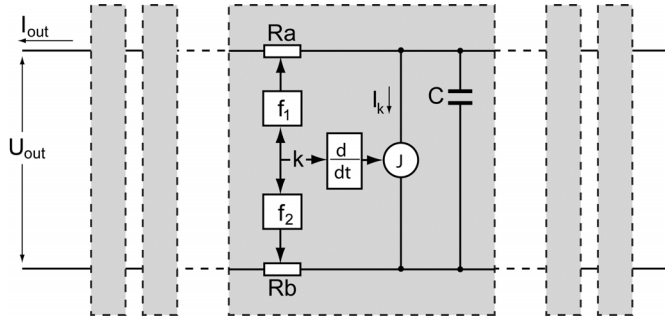

Figure 5.1. Distributed model of IPMC sensor.

As described in Chapter 4, the values of the variable resistors *Ra* and *Rb* depend on the flexure *k* of the IPMC strip at the single unit according to the functions f_1 and f_2 as in the model described in Chapter 4.

The distributed model of IPMC sensor presented in Fig. 5.1. functions in the opposite way compared to the model of an actuator. In the model of the actuator, the electric current through the capacitor C of an elementary unit produces mechanical response k. When a piece of IPMC, utilized as a sensor and represented as a transmission line, is rapidly bent at some region, current I_k is generated in the elementary units of that region by the generators J. The originated electric signals propagate along the IPMC material with finite speed and are suppressed spatially.

In order to demonstrate the damping of the signals, three simulations of the IPMC sensor in different scenarios describing a transitions from one mechanical configuration to another are given.

The scenarios are explained in Fig. 5.2.

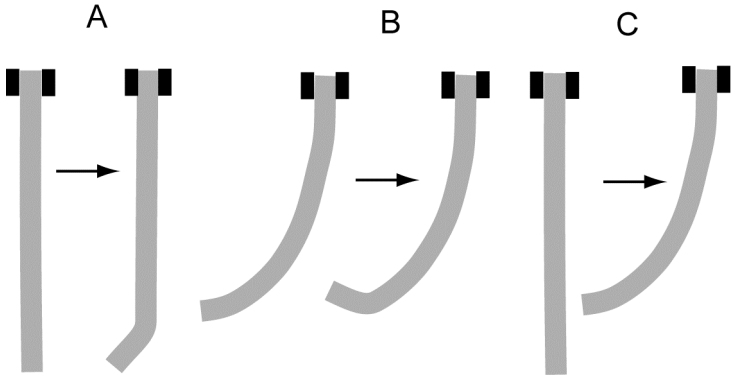

Figure 5.2. The scenarios of the simulations of an IPMC sensor.

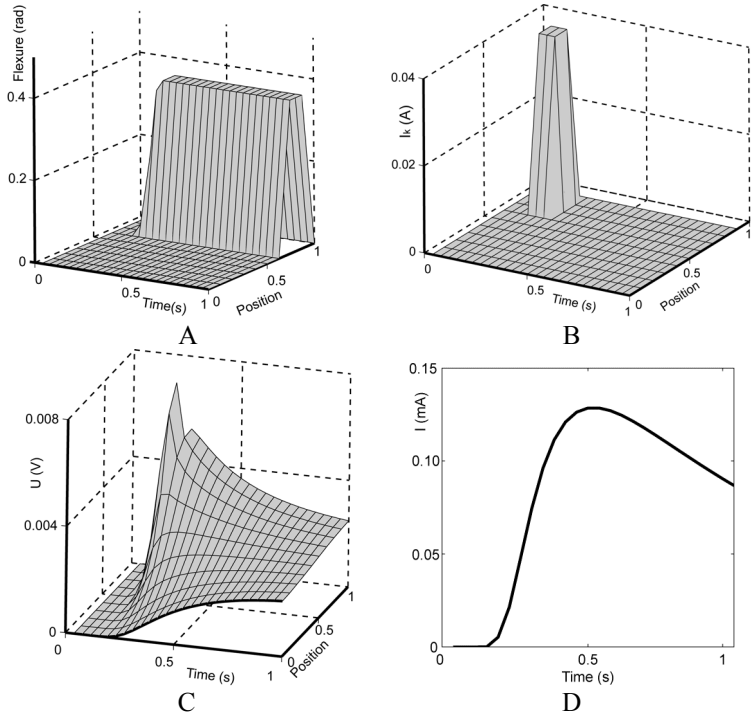

Fig. 5.3. The simulation corresponding to Scenario A.

In Scenario A the initially straight sensor is in a cantilever mode. Only the tip of the sensor moves rapidly during 0.1s at time instance 0.1s. The situation is described in Fig. 5.2.-A. The motion in the form described in Chapter 2.2 is shown in Fig. 5.3.-A. The electric current produced by drift of ions is depicted in Fig. 5.3.-B. This electric current generates a wave of voltage propagating along the IPMC strip, as shown in Fig. 5.3.-C. The voltage at the output of the

sensor U_{OUT} is actually the voltage in Fig. 5.3.-C. at the point, where the relative length is zero. The output current of the sensor I_{OUT} is depicted in Fig. 5.3.-D.

In Scenario B the initial configuration of the sensor differs from the one in A in that the whole strip is initially bent with a constant curvature as shown in Fig. 5.2-B. The relative movement and the induced pulse of electric current are identical to the Scenario A as shown in Fig. 5.4.-A and 5.4.-B respectively. As the resistances of the curved surface electrodes are larger compared to the previous scenario, the propagation of the generated voltage pulse along the length of the sensor is more suppressed. The output voltage and the output electric current are also damped, as seen in Fig. 5.4.-C and 5.4.-D.

In Scenario C the straight strip of the sensor is rapidly bent with a constant curvature as depicted in Fig. 5.2.-C. The motion in the form described in chapter 2.2 and the electric current produced by the drift of ions is presented in Fig. 5.5.-A and Fig. 5.5.-B respectively. As the electric current is produced in the whole device, the produced wave of voltage inside the device is a convolution of all waves generated by all generators of electric current of all single units of the transmission line (Fig. 5.5.-C). The output voltage and the output electric current (Fig. 5.5.-C and Fig. 5.5.-D) express an approximate form of the current caused by the flexure change.

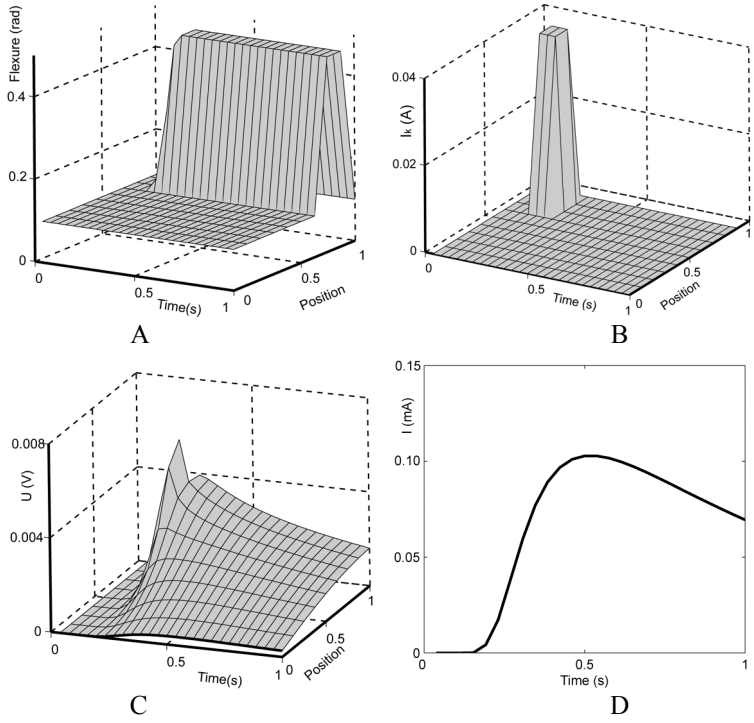

Figure 5.4. Simulation corresponding to scenario B.

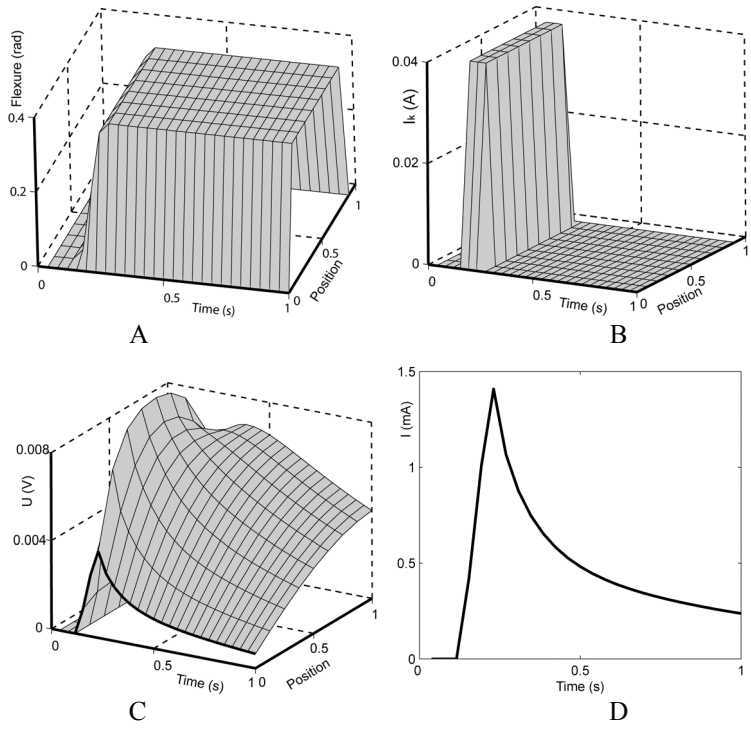

Figure 5.5. The simulation corresponding to Scenario C.

The experimental demonstration of similar situations is described in **I**. The electric signals, generated by an IPMC-based position sensor, were measured at both ends of a pre-bent sensor. A special appliance was made to impose displacement of the middle of the sensor by an electromechanical actuator. If the current is generated at the middle of the sensor, the voltage wave propagates in both directions and generates the output signals of the sensor at both tips of the strip. When the sides were pre-bent differently, the two output signals were damped in a different manner.

The experiments and simulations in some respects confirm the assumption of Farinholt et al. that the output signal of an IPMC sensor is separable as a product of temporal and spatial components [17].

The simulations and experiments show that the output of the IPMC displacement sensors are always delayed and distorted. The extent of distortion increases with the distance between the point of impact and the output contacts. The more the sensor bends, the more the surface resistances increase and therefore the more the output is disturbed.

As a result of the experiments and simulations it can be concluded that the IPMC position sensor is generally capable of detecting the fact of the flexure change only. In order to employ IPMC as a calibrated position sensor, the

mechanical terms should be carefully characterized. Design of such a sensor would imply finding a trade-off between capacity of the IPMC and the signal damping. The smaller is the capacitance of the IPMC the less the signal decays but then the signal generated by the motion is also weaker. In any case, the better is the surface conductivity the better is the sensor. If the external force bending the sensor is large enough, the metal surface electrode should be thick and with a good conductivity.

6. SHUNT CONDUCTIVITY CAUSED BY ELECTRODE REACTIONS

The electrode reactions create additional nonlinearities in the behaviour of IPMC. As described hereinabove, the electrode reactions appear if only the voltage between the electrodes exceeds some certain critical level.

The values of the shunt conductivity resistors can be determined using impedance spectroscopy with variable-voltage step pulses.

The electric current corresponding to a long-lasting step voltage input is depicted in Fig. 6.1. Current peaks sharply at the very first moment (instant A). After charging the whole pseudocapacitor, current remains at a stable level (instant B).

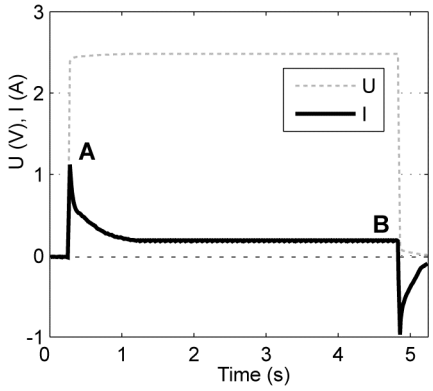

Figure 6.1. Response of the electric current to a rectangular voltage pulse.

This behaviour of current can be explained by analysing the equivalent circuit illustrated in Fig. 6.2. At the very first moment, when the capacitor C is totally discharged, the current flows through the parallel resistances G and Q (instant A). When the capacitance C is totally charged, the current flows through resistance G only (instant B).

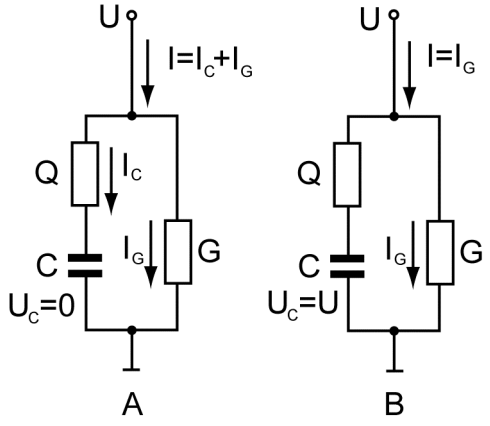

Figure 6.2. Estimation of the resistances G and Q.

The measurements were conducted as follows. A piece of an IPMC with the size of 2 x 10 mm containing Li^+ or Na^+ ions was wholly fixed between gold electrodes. In this configuration the resistance of the electrodes does not influence the results.

Measuring the current at instants A and B (Fig. 6.1.) with voltage pulses of various amplitudes gives a well determined relation between the values of the resistors and the voltage applied as presented in Fig. 6.3 and Fig. 6.4.

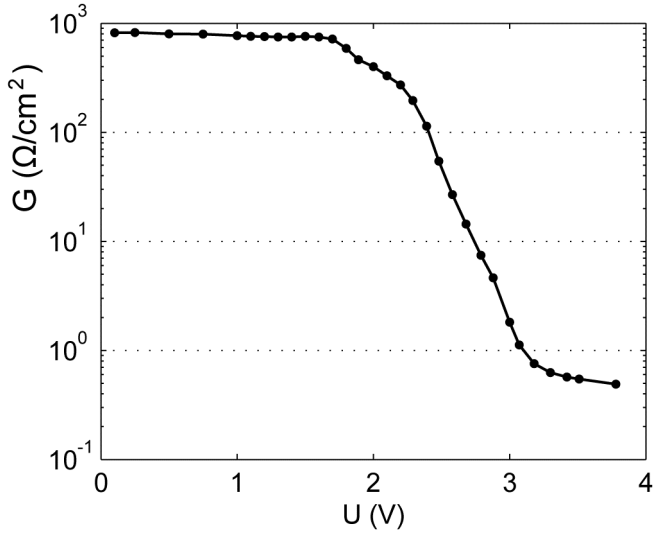

Figure 6.3. The relation between resistance G and the voltage.

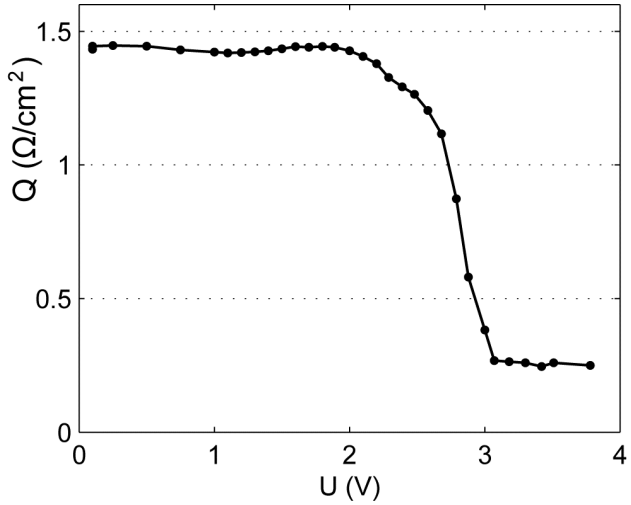

Figure 6.4. The relation between resistance Q and the voltage.

When the voltage is lower than required for water electrolysis, the value of the resistance G is so high that the influence can be neglected and the resistance Q only slightly limits the charging current of the capacitance. Based on these measurements the simplification of the distributed model of the IPMC described in Chapter 3. is justified – if electrolysis does not appear, the resistances Q and G can be disregarded.

When the amplitude of the voltage approaches the voltage required for water electrolysis, both resistances decrease fast, finally reaching very low values: Q~0.1 Ω/cm^2 and G~1 Ω/cm^2. The effect can be explained with electrochemical reactions on electrodes, for example the electrolysis of the solvent. In that case the consumption of electric current and electric power through the resistance G is remarkable. The resistance Q limiting the charging current of capacitance practically disappears, and the performance of an actuator is higher.

The approximate correlation between the values of the resistors and the voltage applied can be characterized empirically with the following equation:

$$R(U) = R_{\infty} + A \cdot (1 - \tanh(B \cdot (U - U_E))), \qquad (6.1)$$

where R_{∞} is the low resistance in case of electrolysis; U_E , A and B are constants. For example G(U) depicted in Fig. 6.3. can be expressed approximately as:

$$G(U) = 1 + 500 \cdot (1 - \tanh(3 \cdot (U - 2.5))). \qquad (6.2)$$

7. A NONLINEAR MODEL CONSIDERING ELECTRODE REACTIONS

The distributed models of IPMC actuators described in chapters 3 and 4 assumed, that the driving input voltages are so low, that the electrode reactions, for example the electrolysis of the solvent, do not appear.

Taking into account the results of characterization of the parameters described in the previous chapter, an improvement can be introduced to the model described in Chapter 4. Additional elements are the two resistors G and Q, shunting the two electrodes of the IPMC in each single unit of the RC transmission line as depicted in Fig. 7.1. The values of G and Q depend on the voltage between the electrodes of the transmission line in that particular single unit, measured by the voltmeter V. The dependence between the voltage $U(x,t)$ and the resistances G and Q can be expressed as in the equation (6.1).

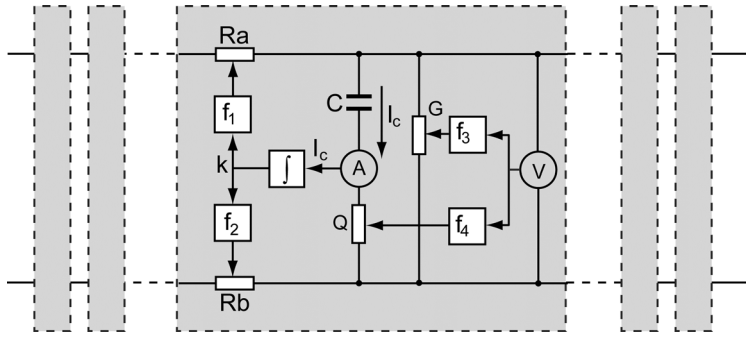

Figure 7.1. A transmission line model considering the electrode reactions.

As it was seen in the previous simulations, the distribution of voltage between the electrodes of the IPMC is usually decreasing along the length due to the voltage drop on the resistance of the electrodes. The influence of the electrode reactions appears only in these regions where the voltage exceeds the critical voltage, whereby the threshold of the critical voltage gradually propagates away from the input contacts.

The resistor Q limits the charging current of the capacitance C. When the electrode reactions appear, the charging current of the capacitance C grows due to the almost disappearing resistance of resistor Q. That in turn increases the actuation capabilities of the device in that region.

The growth of the current I_G through resistor G and the disappearing resistance of resistor Q due to the electrode reactions appear to be very sharp with respect to the voltage. Therefore the equivalent circuit may be approximately divided into two regions composed by different types of single units: the region near the input contacts, where the electrode reactions appear; and the region without electrode reactions, as depicted in Fig. 7.2.

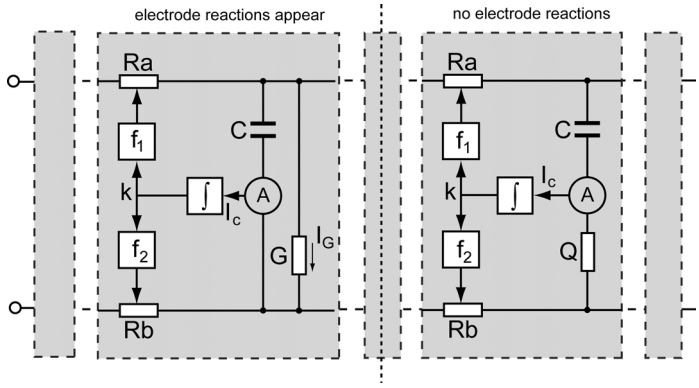

Figure 7.2. Near the input contacts (left) is a region where the electrode reactions appear.

When the electrode reactions appear (the region at left in Fig. 7.2.), the conductivity G grows fast, that in turn affects the power consumption of the device. There will be additional current through the resistors Ra and Rb, causing an additional drop of voltage along the surface electrodes. The voltage between the electrodes diminishes fast to the level, not sufficient for the electrode reactions. The remaining region of the actuator functions as described in Chapter 4 hereinabove.

The mechanical response k of the single units of both regions are calculated by integrating current I_C with respect to time according to the equation (3.9).

The proportional lengths of both regions depend on the resistance of the electrodes and the capacitance of the material. In the experiments conducted by myself, the water electrolysis appeared exclusively between the input contacts and near to the input contacts, as shown in Fig. 2.1.3. and Fig. 1.1., whereas the boundary between the two regions moved slowly away from the contacts. This indicates that the surface resistances of the samples of Musclesheet^{TM} are rather large so that the voltage drops rapidly below the critical level.

8. A SELF-SENSING ACTUATOR

Since IPMC materials exhibit both sensor and actuation properties, a very natural approach would be to use the same material as a position sensor to control the actuator. Several authors have described the constructions where a combination of an IPMC sensor and an IPMC actuator is used for feedback as well as for control. Mallavarapu et al. describe a construction where nonconducting areas are laser-ablated or engraved from the conducting surface coating of an IPMC sheet. As a result a composition of an actuator and a sensor are formed within a single sheet of polymer [50]. Yamakita et al. connect a pair of IPMC films in parallel [66]. Both approaches use one part of the appliance as an IPMC actuator, and another as an IPMC sensor. Then the bending angle of the IPMC actuator is controlled using the estimated value of the bending angle from the sensor system. The problem that arises from this kind of approach is that the output signal of an IPMC sensor is several orders of magnitudes weaker than the driving voltage of the IPMC actuator and the sensor signal gets distorted by the actuator signal and noise [4, 14, **II]**. The current chapter proposes an alternative approach. I describe a self-sensing actuator based on the changing surface resistance of the metal electrodes during the material bending.

While the resistances of the electrodes of the IPMC change in the course of mechanical bending, the behaviour of the voltage drops along the length of the actuator depend on the bending motion of the actuator. The effect is thoroughly described hereabove in chapter 4. The graphs A and C in Fig. 4.3.5. depict the case, when the resistance of the electrodes is invariable; the graphs B and D are the results of simulations, where the resistances of the electrodes change during bending. The experimental results (for example Fig. 2.1.5.) exhibit that actually the voltage behaves similarily to the graphs in Fig. 4.3.5. B and D. The simulated complicated signals presented in Fig. 4.3.5. in fact consist of two components: a component depending on the electrical properties of the material and the component depending on the mechanical shape of the particular piece of the material.

These findings described in the previous chapters have inspired me to develop a simple device that measures the extent of bending by comparing voltage drops on the surfaces. It is thus a self-sensitive actuator, capable of feeling its own motion.

The rest of this chapter describes the device and its working principle.

It is possible to distinguish the two components by taking a longer piece of IPMC for the actuator and assuring, that the resistances of the electrodes of one half of the piece are invariable. It is easy to accomplish by fixing one half of the strip of the IPMC between a clamp as shown in Fig. 8.1. For simplicity we assume, that the length of the fixed and the moving part of the sheet are equal. The acquired actuator has the input contacts in the middle of the strip and feedback contacts at both tips.

The lower half of the actuator depicted in Fig. 8.1. is freely bending; the voltages measured at the lower tips are $UM1$ and $UM2$ (M stands for "Moving"). The upper half is fixed; the voltages measured at the upper tips are $UF1$ and $UF2$ (F stands for "Fixed"). The input driving voltage pulse, fed to the input contacts, propagates towards the "moving" direction as shown in Fig. 4.3.5. B and D as well as towards the "fixed" direction as shown in Fig. 4.3.5. A and C.

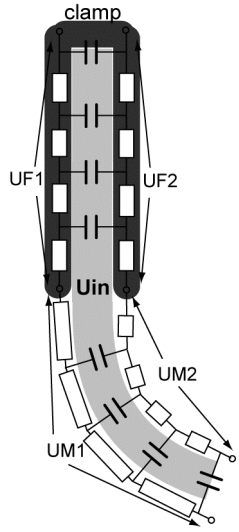

Figure 8.1. The working principle of the self-sensing actuator.

The idea of the self-sensing actuator is to compare the signals $UM1$ and $UM2$ of the moving part to the reference signals $UF1$ and $UF2$ of the fixed tip to determine the extent of bending with respect to the straight sheet. The values of $UF1-UM1$ and $UF2-UM2$ should thus reflect the direction and the extent of bending. The self-sensing actuator can be used in two modes: a surface resistance position sensor and as a self-sensing actuator. In the sensor mode the flexure of the strip can be enquired using short low-voltage pulses at arbitrary moments. In the actuator mode the status of the actuator can be determined analyzing the signals during actuation. The modes can be used alternately by switching between them as needed.

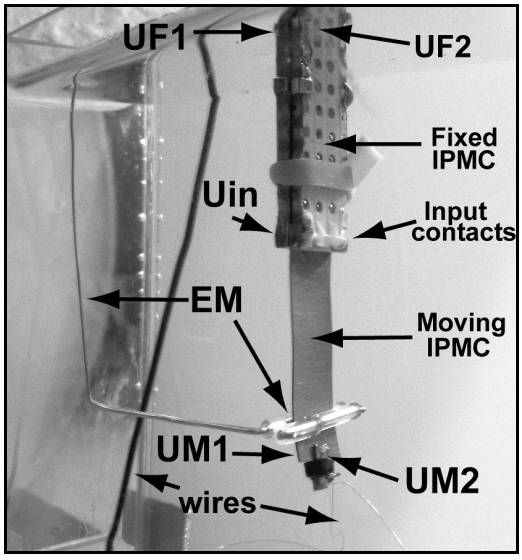

Figure 8.2. The test configuration.

Fig. 8.2. shows the self-sensing actuator in a test configuration. The purpose of the lever driven by an electromechanical actuator (EM) is to apply controlled external force to the IPMC actuator. The EM actuator is controlled by the personal computer (PC).

The experiments with the self-sensing actuator are thoroughly described in **II**.

If desired, the fixed part and the moving part of the actuator may be placed in the same direction from the input contacts, side by side. The essential assumption is, that the electrical properties – resistance of the electrodes and capacitance – of the material are uniform.

In **II** I have shown that the sensor signal of this self-sensing actuator is an order of magnitude stronger compared to the case when the sensor is working as a conventional vibration sensor where the output voltage between the two surface electrodes is recorded.

It can be observed from the experiments that the sensor signals can be easily detected, have a good signal to noise ratio and therefore do not require significant signal preprocessing.

The other advantage is that whereas the conventional vibration sensor works as an accelerometer this sensor also works as a position sensor but can be also used as an accelerometer if the sensor readings are sampled over time. From the application point of view this implies that the sensor readings can be recorded at arbitrary moments, also when the sheet is still.

We also demonstrated that the amplitude of the sensor signal depends on the flexure at any point of the sheet; therefore it is also possible to know more about the position of the actuator than solely the direction of bending.

9. AN S-SHAPE ACTUATOR

The observation that the bending of a relatively long IPMC actuator is faster and stronger close to the input contacts, getting progressively weaker as well as delayed towards the free end of the sheet, motivated me to add additional feeding contacts to the free end of the actuator.

The idea of attaching more contact pairs to an IPMC actuator is not new. Several authors have described the constructions where laser-ablated or engraved nonconducting areas are created in the conducting surface coating. As a result a composition of separate actuators are formed within a single polymer sheet [67, 68, 69]. Attaching the input contacts to the separate areas and driving the separate actuators with different voltages allows to achieve different non-uniform motions of the actuator, for example transferring the bending motion into linear.

As a matter of fact, similar results can be attained using proper timings of the driving voltages within an undivided IPMC sheet. I connected two pairs of contacts to the tips of the actuator as shown in the drawing in Fig. 9.1.-A. The contact $A1$ at the one end of the actuator is connected to the contact $B2$ at the other end of the opposite face. Similarly, the contacts $B1$ and $A2$ connect to the opposite ends at opposite faces. When voltage is applied to the contacts, the ends of the actuator bend towards the opposite directions. Consequently, the whole strip bends like the letter "S", as shown in the schematic in Fig. 9.1.-B and the photo in Fig. 9.2.

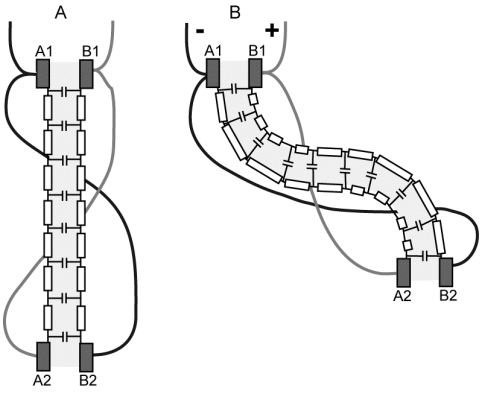

Figure 9.1. Outline of an S-shape actuator.

At the very first moment it may seem that as the resistances of the metal-coated surfaces of the IPMC are low, the S-curved actuator should short-circuit the voltage source via the two parallel metal electrodes. However, this does not happen. The resistances of the surfaces of an unbent actuator are low in fact. As explained in Chapter 4.1 hereinabove, the resistance of the electrodes of IPMC

changes in the course of bending. The inner surface of the IPMC is compressed during bending and its resistance decreases slightly with the decreasing bending radius. The outer surface of a bending IPMC is stretched and its resistance increases several times when the bending radius decreases.

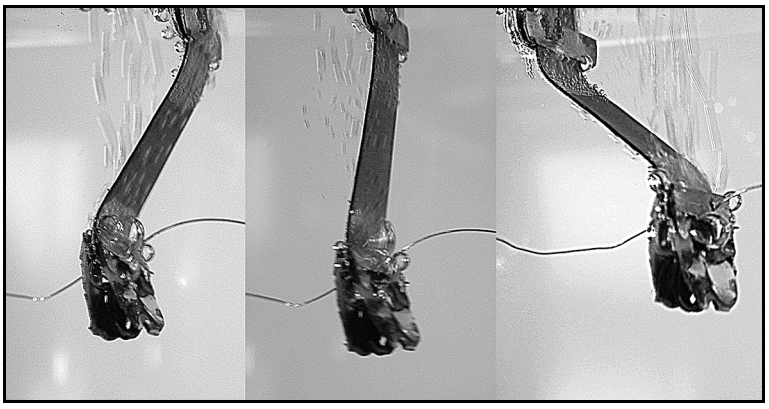

Figure 9.2. The S-shape actuator in a bent configuration with the opposite driving voltage polarities.

The driving voltage has to be increased gradually. As soon a as the actuator starts bending at some occasional region of the actuator, the surface resistance in that region grows and there is no more threat of short-circuiting. From this moment the driving voltage can be increased shortly. The simplified equivalent circuit of the actuator in the bending state looks like in Fig 9.1.-B. The regions with increased and decreased surface resistance are marked as longer and shorter resistors correspondingly. The total resistance of both surfaces is considerable and the amperage of the whole circuit is under control.

The S-shaped actuator uses its resources more efficiently than the “classical” cantilever actuator, actuated from the one end only. The disadvantage of this construction can be the mechanical interference of the wires, increased mechanical complexity in terms of an additional pair of contacts and the weight of the contact clamp. The possible application of this configuration is a linear load-pulling actuator.

It is also possible to feed the contacts at both ends of the actuator with the voltage of the same polarity. As the result both ends of the actuator bend in the same direction.

It has to be pointed out that the force blocking the actuator must be small: if the actuator cannot bend at all, the effect of surface resistance will not appear, and the actuator will still short-circuit the voltage source. It would be useful to implement the feedback of electric current to prevent the damage of the voltage source and the actuator.

10. CONCLUSIONS AND COMMENTS

This thesis presents a novel model of an IPMC. An IPMC is modeled as a distributed RC transmission line. Unlike other electromechanical models of an IPMC, the distributed nature of this model permits predicting the non-uniform bending of the material. Instead of modeling the deflection of the tip of a cantilevered IPMC actuator or sensor without taking an interest in the shape of the device between the tip and the input contacts, this model describes the uneven changing flexion of the device in the time domain.

The main results of this work are:

a) a methodology of characterization of ionic polymer actuators and sensors;
b) a principle of a distributed model of ionic polymer actuators and sensors;
c) an implementation of some possible causes of nonlinearities to the distributed model;
d) two "smart" applications utilizing the distributed model, the self-sensing actuator and an S-actuator.

Chapter 1 provided the background information for ionic polymer materials and discusses some proposed models of actuation. The purpose of this short overview was to demonstrate the variety of possibilities of modelling the electromechanical properties of the material and to bring out the results of other authors, utilized in my own work.

Actually the distributed model of the IPMC introduced in this work uses and elaborates several models discussed in the introduction. It uses the model of Kanno et al. [26] depicted in Fig. 1.8., and extends it as an RC distributed transmission line. The electromechanical coupling between the electric current and flexure change is adapted from the model of Bao et al. [24], and accommodated to the distributed model.

Chapter 2 described the methodology of measuring and graphical representation of the electrical and mechanical characteristics of a bending IPMC cantilever actuator. Actually the methodology is developed as a result of many experiments carried out during the last few years and has been used also by my coworkers and students by carrying out their experiments. The distributed electromechanical model is developed based on these experimental results and also validated using this methodology. Chapter 2. concluded that when the electrical parameters and the changing shape of the IPMC are described in such a specific way, the resemblance between the bending motion and the electrical parameters is apparent.

Chapters 3, 4, 5, and 7 expounded the different modifications of the distributed model of IPMC. Chapter 3 described the simplest model, without any nonlinearities. This is an exceptional case, where a step input to an IPMC-based actuator is solvable in a closed form. All other modifications of the model

are approximated by a lumped RC ladder and modelled with a Matlab Simulink model using the SimPowerSystems toolbox. This toolbox makes it possible to simulate the electrical circuits, using the Kirchhoff's circuit laws. Chapters 4 and 7 introduced the nonlinearities caused by the changing resistance of the electrodes and the water electrolysis respectively. Chapter 5 explained the distributed model of an IPMC sensor, functioning in the opposite way, when compared to the model of an actuator.

It must be pointed out that in the models described in this work, the electromechanical coupling is realized according to the equation (1.6) i.e. without taking into account the relaxation of water back or leakage of water out of from the membrane. Likewise it is possible to implement the more complicated electromechanical coupling, considering these effects, and using the equation (1.5).

The self-sensing actuator described in Chapter 8 and **II** uses the effect of the changing resistance of the electrodes of IPMC. The main advantage of this design is that it can work at the same time as a position sensor, and as an actuator and give a feedback signal from the same actuator. As a disadvantage of this approach it should be mentioned that since the length of the self-sensing actuator is prolonged by the fixed part, the energy consumption of this device is also approximately doubled.

This work describes the behavior of an IPMC as a RC transmission line in time-domain only. The parameters in the frequency-domain, for example the electrical impedance, were not the objective of this work.

For clarity and consistency the experiments and simulations described in this work, are conducted in the case of a rectangular input pulse. However, the model is not limited to the input of that kind. The form of the input signal is not relevant.

The distributed model of an IPMC reported in this thesis represents significant advance in modelling and characterization of ionic polymer transducers. However, several problems deserve further investigation. Some examples are listed below.

The development of the self-sensing actuator is not finished yet. The experiments described in **II** describe only the working principle and represented qualitative results. In order to use the self-sensing actuator in some real-time application, an approximate closed-form solution is required. Likewise the approximate closed-form solutions of the distributed non-linear models described in this work would help to put IPMCs into practice. There exist numerous approximations of the solution of lossy transmission lines in the field of electronics, published during the last half of the last century. Implementing a convenient approximation would help to use IPMCs in real-time applications.

Using some computational electrodynamics modeling technique, for example the finite element method (FEM) or the finite-difference time-domain

method (FDTD) would help to simulate the distributed model better, than the described approximation by a lumped RC ladder.

The described distributed model is only one-dimensional. Simulating the distributed model in two-dimensional space with some computational electro-dynamics modeling technique, would describe the behavior of the IPMC even more accurately.

The distributed model described in this work does not take into account the static mechanical parameters of IPMC membranes, for example the viscoelasticity of polymer membranes, the blocking force produced by the IPMC actuator, inertia, etc. Presumably the combination of the electrical distributed model and the distributed mechanics of composites would give a good result.

REFERENCES

[1] M. Shahinpoor and K. J. Kim, "Ionic polymer–metal composites—I. Fundamentals," Smart Mater. Struct. 10, 2001, pp. 819–833.

[2] S. Nemat-Nasser, C.W. Thomas, "Ionomeric Polymer-Metal Composites", in: Y. Bar-Cohen (Ed.), "Electroactive Polymer (EAP) Actuators as Artifical Muscles. Reality, Potential, and Challenges," SPIE Press, Washington, 2001.

[3] K. J. Kim, "Ionic Polymer-Metal Composite as a New Actuator and Transducer Material," in: "Electroactive Polymers for Robotic Applications. Artificial Muscles and Sensors," Springer-Verlag, 2007, pp. 153–164.

[4] M. Shahinpoor, "Ionic polymer-conductor composites as biomimetic sensors, robotic actuators and artifical muscles – a review," Electrochimica Acta, 48 (2003), pp. 2343–2353.

[5] M. Shahinpoor, "Mechanoelectrical phenomena in ionic polymers," Mathematics and Mechanics of Solids, 8. 2003. pp. 281–288.

[6] K. Oguro, Y. Kawami, and H. Takenaka. "Bending of an ion-conducting polymer film-electrode composite by an electric stimulus at low voltage," Journal of Micromachine Society, 5:27–30, 1992.

[7] K. Sadeghipour, R. Salomon, S. Neogi, "Development of a novel electrochemically active membrane and "smart" material based vibration sensor/ damper," Smart Materials and Structures, Vol. 1, pp. 172–179, 1992.

[8] P. de Gennes, K. Okumura, M. Shahinpoor, K. Kim, Mechanoelectric effects in ionic gels, Europhysics Letters 50 (4) (2000) 513–518.

[9] S. Nemat-Nasser, J. Li, "Electromechanical response of ionic polymer-metal composites," Journal of Applied Physics 87 (7) (2000) 3321–3331.

[10] R. Kanno, A. Kurata, S. Tadokoro, T. Takamori, and K. Oguro. "Characteristics and modeling of icpf actuator," Proceedings of the Japan-USA Symposium on Flexible Automation, pages 219–225, 1994.

[11] K. Asaka, K. Oguro, "Bending of polyelectrolyte membrane platinum composites by electric stimuli. Part II. Response kinetics," Journal of Electroana.ytical Chemistry, 480 (2000), pp. 186–198.

[12] T. Sata. Ion Exchange Membranes. Preparation, Modification and Application. The Royal Society of Chemistry, 2004.

[13] C. Bonomo, L. Fortuna, P. Giannone, S. Graziani, "A method to characterize the deformation of an IPMC sensing membrane," Sensors and Actuators A, 123–124, 2005, pp. 146–154.

[14] C Bonomo, L Fortuna, P Giannone, S Graziani and S Strazzeri, "A model for ionic polymer metal composites as sensors," Smart Mater. Struct. 15 (2006), pp. 749–758.

[15] K. Newbury, and D. Leo, "Linear electromechanical model of ionic polymer transducers – Part I: Model Development," Journal of Intelligent Material Systems and Structures, Vol. 14, No. 6, 2003, pp. 333–342.

[16] C. Bonomo, C.D. Negro, L. Fortuna, S. Graziani, "Characterization of IPMC strip sensorial properties: preliminary results," in: Proc. IEEE ISCAS, 2003, pp. 816–819.

[17] K. Farinholt, D. Leo, "Modeling of electromechanical charge sensing in ionic polymer transducers," Mechanics of Materials, 36 (2004), pp. 421–433.

[18] B. Martin, “Energy harvesting applications of ionic polymers”, Msc. dissertation, Dept. of Mechanical Engineering, Virginia Tech, 2005.
[19] K. Newbury, and D. Leo, “Linear electromechanical model of ionic polymer transducers – part II: experimental validation,” Journal of Intelligent Material Systems and Structures, Vol. 14, No. 6, 2003, pp. 343–357.
[20] K. Newbury, and D. Leo, “Electromechanical modeling and characterization of ionic polymer benders,” Journal of Intelligent Material Systems and Structures, Vol. 13, No. 1, 2002, pp. 51–60.
[21] K. Jung, J. Nam, and H. Choi, “Investigations on actuation characteristics of IPMC artificial muscle actuator,” Sensors and Actuators A: Physical, Vol. 107, No. 2, 2003, pp. 183–192.
[22] S. Nemat-Nasser, and J. Y. Li, “Micromechanics of actuation of ionic polymer-metal composites.” Journal of Applied Physics 92(5), 2002, pp. 2899–2915.
[23] B. Akle, D. Leo, “Electromechanical transduction in multilayer ionic transducers,” Smart Mater. Struct. 13, 2004, pp. 1081–1089.
[24] X. Bao, Y. Bar-Cohen, S. Lih, “Measurements and macro models of ionomeric polymer-metal composites (IPMC),” EAPAD Conference 2002, Proc. SPIE 4695, 2002, pp. 286–293.
[25] C. Bonomo, L. Fortuna, P. Giannone, S. Graziani, S. Strazzeri, “A nonlinear model for ionic polymer metal composites as actuators,” Smart Mater. Struct. 16 (2007) pp. 1–12.
[26] R. Kanno, S. Tadokoro, T. Takamori, M. Hattori, K. Oguro, “Linear approximate dynamic model of an ICPF actuator”, Proc. IEEE Intern. Conf. on Robotics and Automation, Vol. 1, pp. 219–225, Minneapolis, Apr. 1996.
[27] M. Shahinpoor, K.J. Kim, “The effect of surface-electrode resistance on the performance of ionic polymer–metal composite (IPMC) artificial muscles,” Smart Mater. Struct. 9, 2000, pp. 543–551.
[28] M. Shahinpoor and K. J. Kim, “Ionic polymer–metal composites: II. Manufacturing techniques,” Smart Mater. Struct. 12, 2003, pp. 65–79.
[29] D. Bandopadhya, D. Bhogadi, B. Bhattacharya, A. Dutta, “Active vibration suppression of a flexible link using ionic polymer metal composite, IEEE Conference on Robotics, Automation and Mechatronics, Bangkok, 2006.
[30] D. Bandopadhya, B. Bhattacharya and A. Dutta, “An active vibration control strategy for a flexible link using distributed ionic polymer metal composites,” Smart Mater. Struct. 16, 2007, pp. 617–625.
[31] M. Shahinpoor and K. J. Kim, “Ionic polymer–metal composites: IV. Industrial and medical applications,” Smart Mater. Struct. 14, 2005, pp. 197–214.
[32] S. Lee, K. Kim, “Design of IPMC actuator-driven valve-less micropump and its flow rate estimation at low Reynolds numbers,” Smart Mater. Struct. 15, 2006, pp. 1103–1109.
[33] R. Lumia, and M. Shahinpoor, “Microgripper design using electroactive polymers,” In Proc SPIE 2002. on Smart Structures and Materials, California, 1999, Vol. 3669, pp. 322–330.
[34] M. Yamakita, N. Kamamichi, Y. Kaneda, K. Asaka and Z. Luo, “Development of an artificial muscle linear actuator using ionic polymer-metal composites,” Advanced Robotics, 18(4), 2004, pp. 383–399.

[35] N. Kamamichi, Y. Kaneda, M. Yamakita, K. Asaka, and Z. W. Luo, “Biped walking of passive dynamic walker with IPMC linear actuator,” SICE Annual Conference in Fukui, pp. 212–217, August 2003.
[36] J. Rossiter; T. Mukai, “A linear actuator from a single ionic polymer-metal composite (IPMC) strip. Proc. Conf. SPIE EAPAD 2007, to be published.
[37] A. Punning, M. Kruusmaa, A. Aabloo, “S-Shape ionic polymer metal composite actuator,” Conf. Actuator 2006, Bremen, Germany, 14–16 June, 2006. in Proc. pp. 893–895.
[38] T. Fukuda, A. Kawamoto, F. Arai, and H. Matsuura, “Mechanism and swimming experiment of micro mobile robot in water,” in Proc. IEEE Int. Conf. Robotics and Automation, vol.1, 1994, pp. 814–819.
[39] T. Fukuda, A. Kawamoto, F. Arai, and H. Matsuura, “Steering mechanism of underwater micro mobile robot,” in Proc. IEEE Int. Conf. Robotics and Automation, 1995, vol.1, pp.363–368.
[40] S. Guo, T. Fukuda, N. Kato, and K. Oguro, “Development of underwater micro robot using ICPF actuator,” in Proc. IEEE Int. Conf. Robotics and Automation, 1998, pp. 1829–1834.
[41] S. Guo, K. Sugimoto, S. Hata, J.Su, and K. Oguro, “A new type of underwater fish-like micro robot,” in Proc. IEEE Int. Conf. Intelligent Robotics and Systems, 2000, pp. 862–867.
[42] S. Guo, T. Fukuda, and K. Asaka, “Fish-like underwater micro robot with 3 DOF,” in Proc. IEEE Int. Conf. Robotics and Automation, May 2002, pp. 738–743.
[43] S. Guo, T. Fukuda, K. Asaka, “A new type of fish-like underwater microrobot,” IEEE/ASME Transactions on Mechatronics, Vol.8, pp.136–141, 2003.
[44] K. Takagi, Y. Nakabo, Z. Luo, K. Asaka, On a distributed parameter model for electrical impedance of ionic polymer, Proc. Conf. SPIE EAPAD 2007, to be published.
[45] W. Zhang, S. Guo, K. Asaka, “Developments of two novel types of underwater crawling microrobots,” Proc. IEEE Intl. Conf. on Mechatronics & Automation Niagara Falls, Canada July 2005.
[46] Y. Nakabo, T. Mukai, K. Asaka, “Kinematic modeling and visual sensing of multi-DOF robot manipulator with patterned artificial muscle”, Proc. IEEE Int. Conf. Robotics and Automation (ICRA 2005), Barcelona, pp.4326–4331.
[47] J. Rossiter, B. Stoimenov, Y. Nakabo, and T. Mukai: “Three-phase control for miniaturization of a snake-like swimming robot,” IEEE Int. Conf. on Robotics and Biomimetics (ROBIO 2006) (Kunming, 2006.12.17–20), Proc., pp.1215–1220
[48] B. Stoimenov, J. Rossiter, T. Mukai, “Manufacturing of ionic polymer-metal composites (IPMCs) that can actuate into complex curves,” Proc. Conf. SPIE EAPAD 2007, to be published.
[49] K. Mallavarapu, “Feedback control of ionic polymer actuators,” , Msc. Dissertation, Dept. of Mechanical Engineering, Virginia Tech, 2005.
[50] K. Mallavarapu, K. Newbury, and D. Leo, “Feedback Control of the Bending Response of Ionic Polymer-Metal Composite Actuators,” In: Proc. of Smart Structures and Materials 2001 – Electroactive Polymer Actuators and Devices, Vol. 4329, pp. 301–310.

[51] R. C. Richardson, M. C. Levesley, M. D. Brown, J. A. Hawkes, K. Watterson, P. G. Walker, “Control of ionic polymer metal composites,” IEEE/ASME Transactions on Mecatronics, Vol. 8, No. 2, 2003, pp.245–253.
[52] J.-D. Nam, J. H. Lee, J. H. Lee, H. Choe, K. J. Kim, and Y. S. Tak, “Water uptake and migration effects of electroactive IPMC (ion-exchange polymer metal composite) actuator,” Sensors and Actuators A: Physical, Vol. 118, 2005, pp. 98–106.
[53] S. Nemat-Nasser, S. Zamani, “Effect of solvents on the chemical and physical properties of ionic polymer-metal composites,” Journal of Applied Physics 99, 2006, pp. 1–17.
[54] V. Szekely, “Distributed RC Networks,” in “The circuits and filters handbook. 2nd ed.” W. K. Chen (ed) 2003, CRC Press LLC.
[55] V. B. Rao, “Delay analysis of the distributed RC line,” Proc. 32. ACM/IEEE conference on Design automation, p.370–375, June 12–16, 1995, San Francisco, California, United States.
[56] O. Heaviside. Electromagnetic Theory. E.&F.N. SPON LTD, London, 1951.
[57] B. Akle, D. Leo, “Correlation of capacitance and actuation in ionomeric polymer transducers,” Journal of Material Science, 40, 2005, pp. 3715–3724.
[58] M. Anton, A. Aabloo, A. Punning and M. Kruusmaa, “A mechanical model of a non-uniform ionomeric polymer metal composite (IPMC) actuator,” submitted for publication.
[59] M. Anton, A. Aabloo, A. Punning and M. Kruusmaa, “On the optimal design of an ionomeric polymer metal composite (IPMC) actuator,” submitted for publication.
[60] Jezov, “Dynamic measurements of IPMC resistance”, Bsc. dissertation, Dept. of Physics and Chemistry, Tartu University, Tartu, 2006, (in estonian).
[61] E.N. Protonotarios, O. Wing, “Theory of nonuniform RC lines – part I: analytic properties and realizability conditions in the frequency domain,” IEEE Trans. Circuit Theory, vol. CT-14, 1967, pp. 2–12.
[62] E.N. Protonotarios, O. Wing, “Theory of nonuniform RC lines – part II: analytic properties in the time domain,” IEEE Trans. Circuit Theory, vol. CT-14, 1967, pp. 13–20.
[63] E.N. Protonotarios, O. Wing, “Computation of the step response of a general nonuniform RC distributed network,” IEEE Trans. Circuit Theory, vol. CT-14, 1967, pp. 219–221.
[64] K.Singhal, J.Vlach, “Approximation of nonuniform RC distributed networks for frequency- and time-domain computations,” IEEE Trans. Circuit Theory, vol. CT-19, 1972, pp. 347–354.
[65] V.P.Popov, T.A.Bickart, “RC transmission line with nonlinear resistance: large-signal response computation,” IEEE Trans. on Circuits and Systems, vol. CAS-21, 1974, pp. 666–671.
[66] M. Yamakita, A. Sera, N. Kamamichi, K. Asaka and Z. Luo, “Integrated design of IPMC actuator/sensor,” Proc. 2006 IEEE Intl. Conf. on Robotics and Automation, Orlando, Florida, May 2006.
[67] B. Stoimenov, J. Rossiter, T. Mukai, “Manufacturing of ionic polymer-metal composites (IPMCs) that can actuate into complex curves,” Proc. Conf. SPIE EAPAD 2007, to be published.

[68] W. Yim, M. Trabia, J. Renno, K. Kim, Dynamic Modeling of Segmented Ionic Polymer Metal Composite (IPMC) Actuator, Proc of the 2006 IEEE/RSJ Intl Conf on Intelligent Robots and Systems, Oct. 2006, Beijing, China.
[69] Y. Nakabo, T.Mukai, K. Ogawa, N. Ohnishi, K. Asaka, "Biomimetic soft robot using artificial muscle," in Proc. 2004 IEEE/RSJ Intl. Conf. on Intelligent Robots and Systems, Sept. 28 – Oct. 2 2004, Sendai, Japan, in: tutorial WTP3 "Electro-Active Polymer for Use in Robotics"

SUMMARY IN ESTONIAN

Ioonjuhtivatel polümeer-metall-komposiitidel põhinevate tundlike täiturite elektromehhaaniline modelleerimine.

Ioonjuhtiva polümeer-metall-komposiidi (edaspidi IPMC) all mõistetakse tavaliselt elektroaktiivset polümeeri, mis on võimeline painduma elektrivälja toimel. Tegelikult on IPMC mõiste palju laiem. IPMC koosneb ioonvahetuspolümeermembraanist, mis on mõlemalt poolt kaetud elektrit juhtiva metallikihiga e. elektroodiga. IPMC kontekstis olulised komponendid polümeeri stuktuuris on solvent (näiteks vesi), ning kovalentselt seotud anioonsed rühmad, mille laengu kompenseerimiseks on membraanis katioonid. Katioonid on välise elektrivälja toimel võimelised membraanis liikuma. Vee molekulid haakuvad vabade katioonide külge, difundeerudes koos nendega. Kui ühendada elektroodid välise vooluallikaga, siis hakkavad polümeeris olevad katioonid liikuma elektrivälja toimel negatiivse elektroodi suunas, võttes endaga kaasa „hüdraatmantli“ koosseisus olevad vee molekulid. Piltlikult öeldes “pumbatakse” elektrivälja abil katioone koos veega polümeerkile ühe külje ligidusse. Selle tagajärjel membraani üks külg vettib tugevalt ning vastaskülg kuivab kokku, membraan ise paindub kokkukuivava külje suunas. Välise pinge polaarsuse muutumisel paindub IPMC vastassuunas. Toimib ka vastupidine efekt – IPMC-d painutades surutakse vesi koos ioonidega membraani ühe külje suunas. Selle tulemusena tekkinud ebaühtlane ioonide jaotus tekitab elektroodide vahel nõrga pinge. Nii saab IPMC-d kasutada mehhaanilise andurina.

IPMC liigutuse amplituud on suur, kuid tema poolt avaldatav jõud on suhteliselt väike. Elektroodidevaheline pinge, mis on suuteline IPMC-d painutama, on sõltuvalt materjali paksusest mõned voldid, sealjuures on tarbitav voolutugevus tänu materjali suurele ioonjuhtivusele suur. IPMC positsioonianduri väljundpinge on mõni kuni mõnikümmend millivolti. Otsustades viimaste aastate jooksul ilmunud teadusartiklite põhjal, on peamiseks IPMC valmistamiseks kasutatavaks ioonvahetuspolümeeriks Nafion^{TM} ning elektroodimaterjaliks plaatina või kuld.

Esimesed teadusartiklid IPMC kohta avaldati 1990-ndate aastate alguses. Hoolimata umbes 15 aastat kestnud uurimistööst ei ole leitud universaalset mudelit, mis kirjeldaks IPMC-l põhineva täituri liigutuse ning elektriliste sisendsignaalide vahelist seost. IPMC käitumise kirjeldamiseks on erinevad autorid esitanud mitmeid teatud mõttes sarnaseid mudeleid. Nende mudelite sisendparameetriteks on täiturile rakendatav sisendpinge või -vool; väljundparameetriteks aga täituri ühe punkti – enamasti tema otsa – kõrvalekalle algasendist või täituri selle punkti poolt avaldatav jõud. Niisugused mudelid kirjeldavad küll suhteliselt täpselt teatud konkreetse täituri käitumiset, kuid nad ei ole skaleeruvad, s.t. materjali muutudes või täituri mõõtmete muutudes tuleb

mudeli parameetrid uuesti määrata. Võrreldes IPMC-l põhinevaid täitureid käsitlevate uurimistööde arvuga, on IPMC-l põhinevaid andureid kirjeldavaid mudeleid avaldatud palju vähem.

Praegu (aastal 2007) eksisteerivad kõik IPMC rakendused kui prototüübid või teadusprojektid. Ei ole teada ühtki IPMC-l põhinevat seadet.

Käesoleva väitekirja esimene peatükk kirjeldab lühidalt IPMC tööprintsiipi, mõningaid teiste autorite poolt esitatud elektromehhaanilisi mudeleid ning võimalikke rakendusi.

Väitekirja teine peatükk kirjeldab väljatöötatud mõõtmismetoodikat, mis võimaldab täpsemalt määratleda IPMC-l põhinevate täiturite elektrilisi parameetreid ning kuju nende töötamise ajal. Võrreldes teiste autorite poolt kirjeldatud metoodikatega on selles kaks põhilist uuendust:

1. Peale videokaamera abil täituri liigutuse salvestamist ning saadud salvestise iga kaadri töötlemist on võimalik täpselt kirjeldada deformeeruva materjali kuju. Mõõtmistel selgus, et täituri paine on ebaühtlane, sõltudes nii kaugusest sisendklemmidest kui ajast.
2. Kinnitades täituri külge lisaklemme on võimalik mõõta, kuidas muutub pinge täituri elektroodide vahel. Selgus, et ka pinge täituri klemmide vahel on ebaühtlane, sõltudes samuti nii kaugusest sisendklemmidest kui ajast.

Saadud mõõtmistulemustest on näha, et IPMC käitub kui kilekondensaator, mille elektroodidel on halb elektrijuhtivus. Niisugust kondensaatorit on võimalik kirjeldada kui RC transmissiooniliini. Kasutades elektroonikast tuntud pidevate transmissiooniliinide teooriat esitatakse väitekirja 3. peatükis IPMC ühedimensionaalne hajutatud mudel. Seos transmissiooniliini elektriliste parameetrite ja IPMC painde vahel igas mudeli punktis on realiseeritud selles punktis liigutatud laengu hulga kaudu. Esitatud lihtsaim mudel sobib IPMC kirjeldamiseks väikeste painete korral. Selle mudeli peamine oluline uudne omadus on asjaolu, et ta võimaldab välja arendada reaalajas töötavaid IPMC juhtimisalgoritme.

Väitekirja 4. peatükis vaadeldakse IPMC materjali metallelektroodide takistuste sõltuvust paindest ning lisatakse see sõltuvus IPMC hajutatud mudelisse. Mõõtmised näitasid, et IPMC elektroodide juhtivus sõltub materjali paindest. Painutamisel kokkusurutud külje takistus väheneb vähesel määral, väljavenitatud külje takistus suureneb märgatavalt. Niisugune takistuste muutumine mõjutab märkimisväärselt pinge levimist piki transmissiooniliini, seega ka IPMC painde muutumist. Sama efekti rakendatakse 8. peatükis kirjeldatud isetundliku täituri tööpõhimõttes.

Väitekirja 6. ja 7. peatükis näidatakse kuidas elektroodireaktsioonid IPMC metallelektroodidel, näiteks vee elektrolüüs mõjutavad pinge levimist piki transmissiooniliini ning seega ka IPMC käitumist.

Väitekirja 5. peatükk esitab IPMC positsioonianduri ühedimensionaalse hajutatud mudeli. See kirjeldab analoogiliselt eelmistega IPMC-d kui pidevat RC transmissiooniliini, kuid seos anduri painde ja elektriliste väljundsignaalide vahel on realiseeritud hajutatud voolugeneraatorite kaudu. Esitatud simulatsioonid on kooskõlas artiklis **I** kirjeldatud mõõtmistulemustega. Simulatsioonid näitavad, et arvestades materjali suurt mahtuvust ning elektroodide takistuse muutumist materjali painutamisel, on keeruline üheselt kirjeldada IPMC-l põhineva positsioonianduri väljundsignaali.

Väitekirja 9. peatükk kirjeldab mittetraditsioonilist IPMC täiturit. Ühendades täituri sisendsignaali IPMC riba mõlemasse otsa, kuid vastupidise polaarsusega, on võimalik saavutada täituri paindumine kahest otsast S-tähe kujuliselt. Esimesel pilgul võib tunduda, et niisugune ühenamisviis lühistab signaaliallika. Seda ei juhtu, kui materjali paindumisel elektroodide takistus kasvab. Niisugune ühendusviis võimaldab teha tavaliselt painduvast täiturist lineaarse.

Käesolev väitekiri baseerub neljal artiklil ja ühel patenditaotlusel

.

PUBLICATIONS

I

Surface resistance experiments with IPMC sensors and actuators.
A. Punning, M. Kruusmaa, A. Aabloo,
Sensors and Actuators A: Physical, 133/1, 2007, pp. 200–209.

II

A Self-Sensing Ionomeric Polymer Metal Composite (IPMC) Actuator.
A. Punning, M. Kruusmaa, A. Aabloo,
Sensors and Actuators A: Physical, 136/2, 2007, pp. 656–664.

III

A Distributed Electromechanical Model
of Ionomeric Polymer Metal Composite (IPMC).
A. Punning, U. Johanson, M. Anton, A. Aabloo, M. Kruusmaa,
Sensors and Actuators A: Physical, in Print.

IV

Empirical model of a bending IPMC actuator.
A. Punning, M. Anton, M. Kruusmaa, A. Aabloo,
Smart Structures and Materials 2006:
Electroactive Polymer Actuators and Devices (EAPAD);
San Diego, California, USA;
27.02.–02.03.2006. Bellingham: SPIE, 2006,
(Proceedings of SPIE – The International Society
for Optical Engineering), 61681V.

CURRICULUM VITAE

Andres Punning

Sünniaeg ja -koht:	26.01.1961, Valga, Eesti
Kodakondsus:	Eesti
Aadress:	Tartu Ülikooli Tehnoloogiainstituut Nooruse 1, 50411 Tartu, Eesti
Telefon:	+372 737 4832, +372 5 3491976
e-post:	andres.punning@ut.ee

Haridus

1968–1976	Tartu 7. Keskkool
1976–1979	Tartu 1. Keskkool, keskharidus
1979–1984	Tartu Riiklik Ülikool, Füüsika- keemiateaduskonna füüsika eriala

Teenistuskäik

1982–1992	TRÜ Füüsikaosakond teadur
1992–2000	ERA Pank, arvutiinsener
2000–2004	Kaitseväe Ühendatud Õppeasutused, Side- ja IT teenistuse juhataja
2004–2007	Tartu Ülikooli Tehnoloogiainstituut, teadur

Teadustegevus

Polümeersetel aktuaatoritel baseeruvad liikurmehhanismid. Ioonjuhtivate polümeersete metallkomposiitidel (IPMC) baseeruvate aktuaatorite ja sensorite uurimine ning vastavate tehnoloogiate arendamine.

CURRICULUM VITAE

Andres Punning

Date and place of birth:	Jan. 26. 1961, Valga, Estonia
Citizenship:	Estonian
Address:	Tartu University Institute of Technology, Nooruse 1, 50411 Tartu, Estonia
Phone:	+372 737 4832, +372 5 3491976
e-mail:	andres.punning@ut.ee

Education

1968–1976	Tartu Secondary School No. 7.
1976–1979	Tartu Secondary School No. 1.
1979–1984	Tartu State University, Faculty of Physics and Chemistry, specialty of physics

Employment

1982–1992	Tartu University, Dept. of Physics, research fellow
1992–2000	ERA Bank, IT engineer
2000–2004	Estonian National Defence College, Branch of Communications and IT, manager
2004–2007	Tartu University Institute of Technology, research fellow

Scientific work

Research and development of the actuators and sensors based on the Ionic Polymer-Metal Composites (IPMC).

DISSERTATIONES PHYSICAE UNIVERSITATIS TARTUENSIS

1. **Andrus Ausmees.** XUV-induced electron emission and electron-phonon interaction in alkali halides. Tartu, 1991.
2. **Heiki Sõnajalg.** Shaping and recalling of light pulses by optical elements based on spectral hole burning. Tartu, 1991.
3. **Sergei Savihhin.** Ultrafast dynamics of F-centers and bound excitons from picosecond spectroscopy data. Tartu, 1991.
4. **Ergo Nõmmiste.** Leelishalogeniidide röntgenelektronemissioon kiiritamisel footonitega energiaga 70–140 eV. Tartu, 1991.
5. **Margus Rätsep.** Spectral gratings and their relaxation in some low-temperature impurity-doped glasses and chrystals. Tartu, 1991.
6. **Tõnu Pullerits.** Primary energy transfer in photosynthesis. Model calculations. Tartu, 1991.
7. **Olev Saks.** Attoampri diapasoonis voolude mõõtmise füüsikalised alused. Tartu, 1991.
8. **Andres Virro.** AlGaAsSb/GaSb heterostructure injection lasers. Tartu, 1991.
9. **Hans Korge.** Investigation of negative point discharge in pure nitrogen at atmospheric pressure. Tartu, 1992.
10. **Jüri Maksimov.** Nonlinear generation of laser VUV radiation for high-resolution spectroscopy. Tartu, 1992.
11. **Mark Aizengendler.** Photostimulated transformation of aggregate defects and spectral hole burning in a neutron-irradiated sapphire. Tartu, 1992.
12. **Hele Siimon.** Atomic layer molecular beam epitaxy of A^2B^6 compounds described on the basis of kinetic equations model. Tartu, 1992.
13. **Tõnu Reinot.** The kinetics of polariton luminescence, energy transfer and relaxation in anthracene. Tartu, 1992.
14. **Toomas Rõõm.** Paramagnetic H^{2-} and F^+ centers in CaO crystals: spectra, relaxation and recombination luminescence. Tallinn, 1993.
15. **Erko Jalviste.** Laser spectroscopy of some jet-cooled organic molecules. Tartu, 1993.
16. **Alvo Aabloo.** Studies of crystalline celluloses using potential energy calculations. Tartu, 1994.
17. **Peeter Paris.** Initiation of corona pulses. Tartu, 1994.
18. **Павел Рубин.** Локальные дефектные состояния в CuO_2 плоскостях высокотемпературных сверхпроводников. Тарту, 1994.
19. **Olavi Ollikainen.** Applications of persistent spectral hole burning in ultrafast optical neural networks, time-resolved spectroscopy and holographic interferometry. Tartu, 1996.
20. **Ülo Mets.** Methodological aspects of fluorescence correlation spectroscopy. Tartu, 1996.

21. **Mikhail Danilkin.** Interaction of intrinsic and impurity defects in CaS:Eu luminophors. Tartu, 1997.
22. **Ирина Кудрявцева.** Создание и стабилизация дефектов в кристаллах KBr, KCl, RbCl при облучении ВУФ-радиацией. Тарту, 1997.
23. **Andres Osvet.** Photochromic properties of radiation-induced defects in diamond. Tartu, 1998.
24. **Jüri Örd.** Classical and quantum aspects of geodesic multiplication. Tartu, 1998.
25. **Priit Sarv.** High resolution solid-state NMR studies of zeolites. Tartu, 1998.
26. **Сергей Долгов.** Электронные возбуждения и дефектообразование в некоторых оксидах металлов. Тарту, 1998.
27. **Kaupo Kukli.** Atomic layer deposition of artificially structured dielectric materials. Tartu, 1999.
28. **Ivo Heinmaa.** Nuclear resonance studies of local structure in $RBa_2Cu_3O_{6+x}$ compounds. Tartu, 1999.
29. **Aleksander Shelkan.** Hole states in CuO_2 planes of high temperature superconducting materials. Tartu, 1999.
30. **Dmitri Nevedrov.** Nonlinear effects in quantum lattices. Tartu, 1999.
31. **Rein Ruus.** Collapse of 3d (4f) orbitals in 2p (3d) excited configurations and its effect on the x-ray and electron spectra. Tartu, 1999.
32. **Valter Zazubovich.** Local relaxation in incommensurate and glassy solids studied by Spectral Hole Burning. Tartu, 1999.
33. **Indrek Reimand.** Picosecond dynamics of optical excitations in GaAs and other excitonic systems. Tartu, 2000.
34. **Vladimir Babin.** Spectroscopy of exciton states in some halide macro- and nanocrystals. Tartu, 2001.
35. **Toomas Plank.** Positive corona at combined DC and AC voltage. Tartu, 2001.
36. **Kristjan Leiger.** Pressure-induced effects in inhomogeneous spectra of doped solids. Tartu, 2002.
37. **Helle Kaasik.** Nonperturbative theory of multiphonon vibrational relaxation and nonradiative transitions. Tartu, 2002.
38. **Tõnu Laas.** Propagation of waves in curved spacetimes. Tartu, 2002.
39. **Rünno Lõhmus.** Application of novel hybrid methods in SPM studies of nanostructural materials. Tartu, 2002.
40. **Kaido Reivelt.** Optical implementation of propagation-invariant pulsed free-space wave fields. Tartu, 2003.
41. **Heiki Kasemägi.** The effect of nanoparticle additives on lithium-ion mobility in a polymer electrolyte. Tartu, 2003.
42. **Villu Repän.** Low current mode of negative corona. Tartu, 2004.
43. **Алексей Котлов.** Оксианионные диэлектрические кристаллы: зонная структура и электронные возбуждения. Tartu, 2004.

44. **Jaak Talts.** Continuous non-invasive blood pressure measurement: comparative and methodological studies of the differential servo-oscillometric method. Tartu, 2004.
45. **Margus Saal.** Studies of pre-big bang and braneworld cosmology. Tartu, 2004.
46. **Eduard Gerškevitš.** Dose to bone marrow and leukaemia risk in external beam radiotherapy of prostate cancer. Tartu, 2005.
47. **Sergey Shchemelyov.** Sum-frequency generation and multiphoton ionization in xenon under excitation by conical laser beams. Tartu, 2006.
48. **Valter Kiisk.** Optical investigation of metal-oxide thin films. Tartu, 2006.
49. **Jaan Aarik.** Atomic layer deposition of titanium, zirconium and hafnium dioxides: growth mechanisms and properties of thin films. Tartu, 2007.
50. **Astrid Rekker.** Colored-noise-controlled anomalous transport and phase transitions in complex systems. Tartu, 2007.